

RETRIEVING AND MODELLING DIELECTRIC PERMITTIVITY OF DIESEL  
CONTAMINATION IN TERAP RED AND SANDY SOIL USING GROUND  
PENETRATING RADAR

MIMI DIANA BINTI GHAZALI

UNIVERSITI TEKNOLOGI MALAYSIA

RETRIEVING AND MODELLING DIELECTRIC PERMITTIVITY OF DIESEL  
CONTAMINATION IN TERAP RED AND SANDYUSINGSING GROUND  
PENETRATING RADAR

MIMI DIANA BINTI GHAZALI

A thesis submitted in fulfilment of the  
requirements for the award of the degree of  
Doctor of Philosophy (Geomatic Engineering)

Faculty of Built Environment and Surveying  
Universiti Teknologi Malaysia

AUGUST 2022

## **DEDICATION**

To my beloved husband, abah, late mom, son, daughters, brothers and sister.  
Many thanks to Allah for all forgiveness and grace.

## ACKNOWLEDGEMENT

In preparing this thesis, I was in contact with many people, researchers, academicians, and practitioners. They have contributed towards my understanding and thoughts. In particular, I wish to express my sincere appreciation to my main thesis supervisor, Sr. Gs. Dr. Othman Zainon, for encouragement, guidance, critics, and friendship, became the only person who believed in me. I am also very thankful to my co-supervisor, Professor Eng. Dr. Rahmat Mohsin and Dr. Khairulnizam M. Idris for their guidance, advices and motivation. Without their continued support and interest, this thesis would not have been the same as presented here.

The financial support from the Universiti Teknologi MARA (UiTM) and Ministry of Higher Education (MoHE) under the Fundamental Research Grant Scheme (FRGS) for funding my PhD study is acknowledged. Universiti Malaysia Perlis (UniMAP) and UiTM Perlis also deserve special thanks for their assistance in supplying facilities.

My sincere appreciation also extends to all my colleagues, the postgraduate office, and others who have assisted on various occasions. Their views and tips are useful indeed. Special thanks go to Haniyati Ramli, Siti Nor Ain Zainon, Mohd Nazri A Karim and Assoc. Prof. Azremi Abdullah Al-Hadi. Unfortunately, it is not possible to list all of them in this limited space.

I am grateful to all my family members. Special thanks to abah and my late mom for emphasizing the importance of education and all the sacrifice.

Last but surely not least, grateful thanks and appreciation to my beloved husband, Yusmizul Junus, who has “lived” through the writing of this thesis, and whose presence, dedicated love, encouragement, and support, without which none of this could be possible. My love also goes to our daughter and son, Murni AnnurSyuhada, Dahlia Nur Aqilah, Dhiya Nur A’amily, and Aqmal Ziqri, whose wisdom and curiosity serve as a beacon for happiness.

## ABSTRACT

Ground Penetrating Radar (GPR) is a non-destructive, full-wave electromagnetic (EM) measurement tool for quantitative imaging to describe dielectric permeability distributions. It is an efficient technique for detecting diesel contamination in soil tomography problems. However, dielectric permittivity relies entirely on variance moisture content facilitated by diesel fuel reaction soil, which determines GPR velocity. Difficulties in interpreting GPR reflection configuration are complex qualitative features limited to noisy or nonlinear relations problems. Consequently, positioning and depth determination would be misleading due to severe polarization and velocity mismatch in traveling-wave typically in Terap Red soil as silty-clay soil. Therefore, this study aims to determine the mathematical model for dielectric permittivity prediction and investigate the GPR signal segmentation algorithm model to map the diesel contamination plume in Terap Red soil. The calibration icon function of the GPR signal was quantified by dielectric permittivity prediction. The research approach was divided into 4 phases. The investigation commenced with an evaluation of the GPR propagation signal from a simulated diesel contamination plume of Terap Red and sandy soils concerning the results of geotechnical measurements using BS 1337: 1992. Next, the dielectric permittivity using the GPR velocity in modeling the empirical relationship between dielectric permittivity and moisture content was determined using statistical analysis. Additionally, cross-validation was performed using existing literature, Vector Network Analyzer (VNA) and in-situ measurements before the GPR signal images were segmented and categorized using a Support Vector Machine (SVM). Finally, ten-fold cross-validation and Logistic Regression (LR) classification were used to evaluate the spatial distribution classification mapping of GPR signals. The result shows the best prediction on Terap Red soil from third-order polynomial using ANOVA yielded a strong positive correlation ( $R^2=0.9892$ ,  $N=24$ ,  $P < 0.05$ ) and a standard error of 0.076. The accuracy of dielectric permittivity in terms of root mean square error (RMSE) and mean absolute error (MAE) was obtained at  $9.772E-14$  and 0.049, respectively. The best-fitting relationship does exhibit some degree of textural bias that should be considered in the choice of petrophysical relationship with uncertainty mean differences via VNA validation for Terap Red and sandy soil were only 2.706 % and 1.985 %, compared to over 3.608% and 15.990 % for the existing model. The accuracy of the spatial distribution classification map generated by the SVM classifier is encouraging, with RMSE of 0.139, kappa statistics of 0.888, and correct instances classified (CIC) of nearly 100 % for both SVM and LR. In conclusion, the study results on dielectric permittivity prediction of contaminated soils for Terap Red and sandy soils indicate that the empirical relationship model is only applicable to specific soils with similar properties. Additional supervised data is recommended to achieve better classification outputs.

## ABSTRAK

Radarm Penembusan Tanah (GPR) adalah alat pengukuran tanpa kerosakan, pengukurannya berasaskan gelombang elektromagnetik gelombang penuh (EM) untuk pencitraan kuantitatif bagi menerangkan taburan ketelusan dielektrik dan teknik yang cekap mengesan pencemaran diesel dalam masalah tomografi tanah. Walau bagaimanapun, ketelusan dielektrik bergantung sepenuhnya pada kepelbagaian kelembapan yang didorong oleh tanah reaksi bahan bakar diesel, yang mana digunakan untuk menentukan halaju GPR. Penafsiran konfigurasi refleksi GPR adalah sukar kerana ciri kualitatif yang kompleks, yang mana terhad kepada masalah hingar atau hubungan tidak linear. Oleh sebab itu, kesilapan penentuan kedudukan dan kedalaman mungkin berlaku disebabkan polarisasi yang teruk dan ketidaksepadan halaju dalam perjalanan-gelombang terutama pada tanah Terap Red sebagai tanah halus-liat. Maka, kajian ini bertujuan untuk menentukan model matematik untuk meramal permitiviti dielektrik dan menyiasat model algoritma bagi segmentasi isyarat GPR untuk memetakan kosentrasi pencemaran diesel di tanah Terap Red. Ramalan permitiviti dielektrik telah digunakan sebagai fungsi penentuan isyarat GPR. Pendekatan kajian dibahagikan kepada empat (4) fasa. Penyiasatan dimulakan dengan penilaian isyarat penyebaran GPR daripada simulasi pencemaran diesel tanah Terap Red dan tanah berpasir berhubung dengan keputusan pengukuran geoteknikal menggunakan BS 1337: 1992. Seterusnya, penentuan ketelusan dielektrik menggunakan halaju GPR dalam memodelkan hubungan empirikal antara ketelusan dielektrik dan kandungan lembapan menggunakan instrumen analisis statistik. Selain itu, pengesahan silang dilakukan menggunakan literatur sedia ada, Penganalisis Rangkaian Vektor (VNA) dan pengukuran di tapak sebelum imej isyarat GPR disegmenkan dan dikategorikan menggunakan Mesin Vektor Sokongan (SVM). Pengesahan 10 kali ganda dan pengelasan Regresi Logistik (LR) telah digunakan untuk menilai pemetaan klasifikasi taburan spatial isyarat GPR. Keputusan menunjukkan ramalan terbaik pada tanah Terap Red daripada polinomial tertib ketiga menggunakan ANOVA menghasilkan korelasi positif yang kuat ( $R^2 = 0.9892$ ,  $N = 24$ ,  $P < 0.05$ ) dan ralat piawai 0.076. Ketepatan permitiviti dielektrik dari segi ralat punca min punca (RMSE) dan ralat mutlak min (MAE) diperoleh masing-masing pada  $9.772E-14$  dan 0.049. Hubungan model yang paling sesuai menunjukkan tahap kecenderungan tekstur harus dipertimbangkan dalam memilih hubungan petrofisik melalui perbezaan min ketidaktentuan daripada pengesahan VNA untuk tanah Terap Red dan berpasir hanya 2.706% dan 1.985%, berbanding melebihi 3.608% dan 15.990% untuk model sedia ada. Ketepatan peta klasifikasi taburan spatial menggunakan pengelasan SVM adalah memberangsangkan, dengan RMSE, 0.139, statistik kappa, 0.885 dan Perkelas Contoh Betul (CIC) pada kadar hampir 100% untuk kedua-dua SVM dan LR. Kesimpulannya, hasil kajian ramalan kebolehtelapan dielektrik bagi tanah tercemar bagi tanah Terap Red dan berpasir menunjukkan bahawa model hubungan empirikal hanya terpakai untuk tanah tertentu dengan ciri-ciri yang sama. Data diselia tambahan yang lebih banyak disarankan untuk mencapai hasil kejituan klasifikasi yang lebih baik

## TABLE OF CONTENTS

	<b>TITLE</b>	<b>PAGE</b>
	<b>DECLARATION</b>	<b>iii</b>
	<b>DEDICATION</b>	<b>iv</b>
	<b>ACKNOWLEDGEMENT</b>	<b>v</b>
	<b>ABSTRACT</b>	<b>vi</b>
	<b>ABSTRAK</b>	<b>vii</b>
	<b>TABLE OF CONTENTS</b>	<b>viii</b>
	<b>LIST OF TABLES</b>	<b>xiii</b>
	<b>LIST OF FIGURES</b>	<b>xvi</b>
	<b>LIST OF ABBREVIATIONS</b>	<b>xxiv</b>
	<b>LIST OF SYMBOLS</b>	<b>xxvi</b>
	<b>LIST OF APPENDICES</b>	<b>xxix</b>
<b>CHAPTER 1</b>	<b>INTRODUCTION</b>	<b>1</b>
	1.1 Research Background	1
	1.2 Problem Statement	6
	1.3 Objectives	8
	1.4 Significance of the Study	8
	1.5 Scope and Limitation	9
	1.6 Thesis Outline	10
<b>CHAPTER 2</b>	<b>LITERATURE REVIEW</b>	<b>11</b>
	2.1 Introduction	11
	2.2 Soil Properties	12
	2.2.1 Terap Red soil	17
	2.3 Soil Contamination by Diesel	19
	2.3.1 Diesel Fuel	23
	2.4 Detection of LNAPL-Contaminated Soil	25

2.4.1	Geotechnical Methods for Soil Contamination Identification	26
2.4.1.1	Grain Size Distribution	29
2.4.1.2	Atterberg Limit	30
2.4.1.3	Determination of Soil Density	34
2.4.2	Geophysical Methods for Soil Contamination Identification	36
2.5	Ground Penetrating Radar for Soil Contamination Identification	38
2.5.1	Type and Configuration of Ground Penetrating Radar	44
2.5.2	Frequencies of GPR and Depth of Detection and its Application	49
2.5.3	Sampling Frequency	52
2.5.4	Sampling Density	53
2.5.5	Stacking	54
2.5.6	Trigonometry Interval	55
2.6	Prediction Dielectric Permittivity Equation	57
2.6.1	Statistical Analysis of an Empirical Equation	60
2.7	Evaluation Method	63
2.8	Automated Classification Mapping	67
2.9	Summary	69
<b>CHAPTER 3</b>	<b>RESEARCH METHODOLOGY</b>	<b>71</b>
3.1	Introduction	71
3.2	Research Design	71
3.3	Simulation of Soil Diesel Contamination	75
3.4	Data Collection	80
3.4.1	GPR Calibration	80
3.4.2	GPR Data Collection	81
3.4.3	Soil Moisture Test	86
3.4.4	Geotechnical Test	88
3.4.4.1	Sieve Analysis (Grain Size Analysis)	89



	3.4.4.2	Atterberg Limits	91
	3.4.4.3	Determination of Density	96
3.5		Post Processing and Accuracy Evaluation of GPR Signal Image	97
	3.5.1	GPR Basic Processing	98
		3.5.1.1 Time Zero Correction	99
		3.5.1.2 Dynamic Correction	100
		3.5.1.3 Background Removal	102
		3.5.1.4 De-wow Filtering	103
		3.5.1.5 Bandpass Filtering	104
		3.5.1.6 Gain Function	106
		3.5.1.7 Hyperbola Fitting	109
	3.5.2	Accuracy Assessment GPR Data Processing	110
3.6		Data Interpretation and Empirical Relationship Modelling	111
	3.6.1	Data Interpretation and Analysis of Diesel Contamination	112
		3.6.1.1 Calculation of Soil Dielectric Permittivity from GPR Signal	112
		3.6.1.2 Statistical of Empirical Analysis	113
	3.6.2	Accuracy Assessment of Empirical Model	114
	3.6.3	Verification of Predicted Dielectric Permittivity	114
3.7		Automated Classification Mapping using Support Vector Machine	121
3.8		Summary	122
<b>CHAPTER 4</b>		<b>RESULT AND ANALYSIS</b>	<b>125</b>
	4.1	Introduction	125
	4.2	Accuracy Assessment of GPR Image for Contaminated soil	126
	4.3	Interpretation of GPR Image for Contaminated Soil	129
		4.3.1 Interpretation of GPR Image for Diesel Contaminated in Terap Red Soil	130
		4.3.2 Interpretation of GPR Image for Diesel Contaminated in Sand Soil	136

4.4	The Influence of Diesel Contamination on EM Velocity and Dielectric Permittivity	141
4.4.1	The Influence of Diesel Contamination on EM Velocity and Dielectric Permittivity in Terap Red Soil	141
4.4.2	The Influence of Diesel Contamination on EM Velocity and Dielectric Permittivity in Sandy Soil	144
4.5	The Association between Soil Moisture Content and Dielectric Permittivity in Contaminated Soil	147
4.5.1	The Association between Soil Moisture Content and Dielectric Permittivity in Terap Red Contaminated Soil	148
4.5.2	The Association between Soil Moisture Content and Dielectric Permittivity in Sandy Contaminated Soil	150
4.6	Model Fitting of Empirical Relationship Model between Moisture Content and Dielectric Permittivity	155
4.6.1	Model Fitting Empirical Relationship Model between Moisture Content and Dielectric Permittivity for Contaminated Terap Red Soil	156
4.6.2	Model Fitting Empirical Relationship Model between Moisture Content and Dielectric Permittivity for Contaminated Sandy Soil	163
4.7	Validation of the Observed Data and Predicted Dielectric Permittivity	172
4.7.1	Validation of the Observed Data and Predicted Dielectric Permittivity for Contaminated Terap Red Soil	173
4.7.2	Validation of the Observed Data and Predicted Dielectric Permittivity for Contaminated Sandy Soil	179
4.8	GPR Signature Segmentation for Classification Model Mapping of Contaminated Soil by Support Vector Machine (SVM)	187
4.9	Verification of In-situ Observation and Predicted Dielectric Permittivity for Contaminated Terap Red soil with SVM Classification Model Mapping	195
4.10	Summary	198

<b>CHAPTER 5</b>	<b>CONCLUSION AND RECOMMENDATION</b>	<b>199</b>
5.1	Introduction	199
5.2	Specific Conclusion and Contribution	200
5.3	Research Limitation	204
5.4	Recommendation	204
<b>REFERENCES</b>		<b>207</b>
<b>LIST OF PUBLICATIONS</b>		<b>280</b>

## LIST OF TABLES

<b>TABLE NO.</b>	<b>TITLE</b>	<b>PAGE</b>
Table 1. 1	Emission factor for stationary combustion in the energy sector based on kg of greenhouse gas per TJ on a Net Calorie Basis, according to the IPCC report (Latif et al., 2021)	3
Table 2. 1	List of past and recent studies (up to the year 2021) for contamination by various types of LNAPL in various soil properties of different classifications	22
Table 2. 2	Properties of diesel fuel and other fuels	24
Table 2. 3	Review of research study on soil contamination by LNAPLs based on geotechnical method	28
Table 2. 4	Factors affecting the liquid limit test with a one-point cone penetrometer (adopted: BS 1377-2 (1990))	32
Table 2. 5	Factors affecting a single point method of the casagrande apparatus for determining the liquid limit (adopted: BS 1377-2 (1990))	32
Table 2. 6	Review of research study on Soil Contamination by LNAPLs using GPR	42
Table 2. 7	GPR depth detection capabilities depend on the frequency and applications, including GPR signal processing software.	51
Table 2. 8	Stacking step for a total of 4 signal traces in a single record with a signal to noise data (red number); the improvement of SNR from the nearest integer rounding (blue number) from the average signal amplitude (green number).	55
Table 2. 9	List of Applications for the existing dielectric permittivity prediction model	58
Table 2. 10	Degree of correlation coefficient (modified from Chua, 2006)	62
Table 3. 1	GPR processing parameters used for laterite soil scanning	84
Table 3. 2	The differences in moisture content, $\theta$ (%) between moisture content probe test and oven-dried method (laboratory test) for two types of soil (i) Terap Red soil and (ii) Sand	88

Table 3. 3	Mass of soil sample for sieving (BS 1377-2:1990)	90
Table 3. 4	GPR processing parameters used for Terap Red soil scanning with Reflexw Software.	99
Table 4. 1	Descriptive accuracy evaluation value for the GPR profile validation component for soils in clean and contaminated conditions.	129
Table 4. 2	The reflection coefficient (R) of GPR signal in radar facies on contaminated Terap Red soil	132
Table 4. 3	The soil properties of the liquid limit, plastic limit and plasticity index for Terap Red soil and Sand soil in both conditions are clean and contaminated.	134
Table 4. 4	Compositions in Percent by Weight Medium in BS Soil Classification for Terap Red soil and Sandy soil	135
Table 4. 5	Moisture content of both types of soil using Oven-Dried method in Laboratory Test	138
Table 4. 6	The reflection coefficient (R) of GPR signal in radar facies on contaminated sandy soil.	139
Table 4. 7	Physical properties of soil test (Density and Porosity)	145
Table 4. 8	The descriptive statistics of the dielectric permittivity based on soil moisture test for the processed GPR data on Terap Red diesel contaminated soil	150
Table 4. 9	The descriptive statistics of the dielectric permittivity based on soil moisture test for the processed GPR data on sandy diesel contaminated soil	154
Table 4. 10	Model summary of empirical relationship model of Contaminated Terap Red Soil	158
Table 4. 11	A summary of empirical relationship model outputs and ANOVA analysis for Contaminated Terap Red soil	158
Table 4. 12	Summarises the Best-Fit model by the third-order polynomial coefficient analysis for contaminated Terap Red soil	159
Table 4. 13	A summary of comparison and accuracy between $\epsilon_r$ predicted and $\epsilon_r$ measured for all regression analyses (fitted-model) for contaminated Terap Red soil	163
Table 4. 14	Model summary of empirical relationship model of contaminated sandy soil	165
Table 4. 15	A summary of empirical relationship model outputs and ANOVA analysis of contaminated sandy soil	166

Table 4. 16	A summary of the Best-Fit model by the third-order polynomial coefficient analysis for contaminated sandy soil	167
Table 4. 17	A summary of comparison and accuracy between $\epsilon_r$ predicted and $\epsilon_r$ measured for all regression analyses (fitted-model) on contaminated sandy soil.	171
Table 4. 18	A statistic summary of predicted dielectric permittivity value and RMSE accuracy using all empirical models, GPR measured data and calibrated VNA for contaminated Terap Red soil	174
Table 4. 19	A summary of comparison and accuracy between $\epsilon_r$ predicted and $\epsilon_r$ measured for Best-Fit model, Topp model and CRIM model on contaminated Terap Red soil	175
Table 4. 20	A summary of dielectric permittivity comparison between min, max, the mean and standard deviation of $\epsilon_r$ VNA with measured data, Best-Fit model, Topp model and CRIM model on contaminated Terap Red soil	178
Table 4. 21	A statistic summary of predicted dielectric permittivity value and RMSE accuracy using all empirical models, GPR measured data and calibrated VNA for contaminated sandy soil	181
Table 4. 22	A summary of comparison and accuracy between $\epsilon_r$ predicted and $\epsilon_r$ measured for Best-Fit model, Topp model, and CRIM model for contaminated sandy soil	183
Table 4. 23	A summary of dielectric permittivity comparison between min, max, a mean and standard deviation of $\epsilon_r$ VNA with measured data, Best-Fit model, Topp model, and CRIM model for contaminated sandy soil	185
Table 4. 24	Summarises the classification model's accuracy using polykernel in the SVM classifier for contaminated Terap Red and sandy soil	189
Table 4. 25	Summarises the classification model's accuracy using the LR classifier for contaminated Terap Red and sandy soil	190
Table 4. 26	Summarises the classification model's accuracy using the LR classifier for contaminated Terap Red and sandy soil	196

## LIST OF FIGURES

<b>FIGURE NO.</b>	<b>TITLE</b>	<b>PAGE</b>
Figure 1. 1	The molecular mechanism of typical pulmonary lesions induced by DEP and SARS-CoV-2 exposure in the environment, adopted from (Mustafa et al., 2020)	2
Figure 1. 2	Percentage of energy source inputs used in power plants (Latif et al., 2021)	3
Figure 2. 1	The four components of soil by volume. (Adapted from Brady and Weil, 2002)	13
Figure 2. 2	The soil composition. Soil organic matter and minerals make up the solid fraction, whereas water and air comprise the pore space fraction	13
Figure 2. 3	The textural triangle represents the relative composition of sand, silt, and clay in soil type classification (Adapted from Rhodes, 2013)	14
Figure 2. 4	Basic types of soil structure: (a) Granular, (b) blocky, (c) prismatic, and (d) massive (modified from Rai et al., 2017).	15
Figure 2. 5	View of soil ranging from very low porosity/permeability to high porosity/permeability	16
Figure 2. 6	Generalise Soil Map in Northern Malaysia published by Ministry of Agriculture and Food Industries (1970)	18
Figure 2. 7	Variation viscosity of Diesel fuel concerning temperature, adapted from Schaschke et al. (2013)	20
Figure 2. 8	Variation viscosity of kerosene concerning temperature, adapted from Mao et al. (2017)	21
Figure 2. 9	Total annual liquid production and consumption in Malaysia (thousand barrels per day) (U.S. Energy Information Administration, 2021)	25
Figure 2. 10	Soil particles before and after LNAPL contamination (modified from Khoshgoftar et al., 2021)	27
Figure 2. 11	Range mass of sample required for particle size distribution by sieve analysis test by BS Soil Classification 1377-2: 1990	30

Figure 2. 12	Setup diagram for time-domain reflectometry (TDR) acquisition. (a) Soil column equipped with a TDR probe; (b) data logger; and (c) external Personal Computer (PC) for data processing (Vergnano et al., 2019)	37
Figure 2. 13	The ERT principle is based on the difference between two electrodes: current and potential (Hung et al., 2019)	38
Figure 2. 14	Ground-couple GPR Equipment: MALA Pro-Ex	39
Figure 2. 15	GPR reflected amplitude (modified from A. Benedetto & Benedetto, 2014)	40
Figure 2. 16	Schematic diagram of the geometry of the GPR survey (modified from Lai et al. (2016) )	43
Figure 2. 17	Schematic of GPR complete hyperbola	44
Figure 2. 18	Schematic signal reflection from two type of GPR : (a) air-coupled GPR and (b) ground-coupled GPR ( modified from To, 2013)	45
Figure 2. 19	GPR measurement of asphalt pavement using an air-coupled with horn antenna (modified from Liu et al., 2017)	46
Figure 2. 20	Antenna separation (s) as a distance separation between the receiver and the transmitter for fixed shielded wideband antennas in the common-offset method	47
Figure 2. 21	Antenna separation (s) as a distance separation between the receiver and the transmitter for fixed shielded wideband antennas in the common mid-point method	48
Figure 2. 22	Antenna separation (s) as a distance separation between the receiver and the transmitter for fixed shielded wideband antennas in the common mid-point method	49
Figure 2. 23	The occurrence of wavelengths in the detection of two neighboring objects: high frequency and low frequency	50
Figure 2. 24	Sampling frequency techniques: Comparison of the reconstructed signal from insufficient sampling frequency towards the original signal (revised from Cornforth et al., (2018)	52
Figure 2. 25	An original sinusoidal signal quantized using 8 bits and 64 bits (revised from Cornforth et al., (2018)	54
Figure 2. 26	Modelling of the sinusoidal waveform in a trigonometric function	56
Figure 2. 27	Sinusoidal waveform for the linear wave equation	56



Figure 2. 28	SVM hyperplanes for a non-separable data set (Verma et al., 2018)	68
Figure 3. 1	Flowchart of research methodology	74
Figure 3. 2	Detail flow chart of the testbed construction for simulation of the soil diesel contamination	75
Figure 3. 3	Model of simulation leakage tank (a) Outside view and dimension of tank constructed by concrete (b) Inside view from front and side view of tank with height of simulation leakage was buried	77
Figure 3. 4	Design of simulation leakage tank using concrete block and plywood partition	78
Figure 3. 5	Design of simulation leakage tank divided by two (2) partitions and filled with two (2) types of soil: (a) Terap Red soil (Lateritic soil type) and (b) Sand soil	78
Figure 3. 6	The simulation pipe leakage: (a) Location of pipe buried in soil tank in 0.5m depth and (b) the hole measurement on PVC pipe for diesel leakage	79
Figure 3. 7	Flow Chart of Detail Methodology for Data Collection	80
Figure 3. 8	The GPR measurement; gridline with the interval of 0.5 m for each grid and scanning direction in which L1 and L2 represent Longitudinal scanning line while T1, T2, and T3 represent Traversal scanning line	83
Figure 3. 9	GPR measurement (a) Traversal line measurement and (b) Longitudinal line measurement	83
Figure 3. 10	The point of soil moisture test measurement (red dot point) along the GPR profile line with a 0.25m interval	87
Figure 3. 11	The soil moisture test measurement; (a) soil moisture test point (red dot point) along GPR profile line with 0.25m interval and (b) the measurement of soil moisture probe during GPR measurement	87
Figure 3. 12	Volumetrics moisture content test by the oven-dried method for 5kg of soil sample (a) Terap Red soil and (b) Sandy soil	88
Figure 3. 13	Classification of soil by a sequence of sieve set containers on a sieve shaker in compliance with BS Classification 1377-2:1990	90
Figure 3. 14	Soil retained after 15 minutes of sieve shaking: (a) before sieve (b) after sieve	91

Figure 3. 15	Liquid limit test following Casagrande Method in BS Classification Soil 1377-2:1990: (a) Soil paste of Terap Red Soil and (b) Liquid limit test using Grooving Tool and Gauge	93
Figure 3. 16	The soil pastes of Terap Red and Sand after liquid limit and plastic limit test (before oven-dried)	94
Figure 3. 17	Soil sample paste in the plastic limit test for Terap Red soil	95
Figure 3. 18	The plastic limit test procedure	95
Figure 3. 19	The moisture content measurement for plastic limit sample result	96
Figure 3. 20	Particle density test	97
Figure 3. 21	Bulk density test	97
Figure 3. 22	Detail Steps of Data Processing and Accuracy Evaluation for GPR signal image	98
Figure 3. 23	Time-delayed was omitted from GPR raw data, and the amplitude in the blue box shows the A-Scan of the GPR signal image, which modified the depth shift more precisely	100
Figure 3. 24	The GPR signal image shows no significant change following the dynamic correction process	101
Figure 3. 25	The GPR signal image with background noise (before applying the background removal) and clean data (after using background removal to all whole lines)	102
Figure 3. 26	DC bias and very low-frequency signal trend in the data shows as ‘wow’ effect and GPR data-trace after de-wow filtering	103
Figure 3. 27	Low-frequency components in GPR data were extracted during the de-wow process, which was performed in a time domain and represented in a single GPR trace (blue box)	104
Figure 3. 28	Frequency domain bandpass filter	105
Figure 3. 29	GPR signal image was enhanced in specific amplitude ranges and visually improved after applying the bandpass filter	106
Figure 3. 30	Spherical divergence of GPR signal	107
Figure 3. 31	The power gain function to compensate for the signal attenuation	108

Figure 3. 32	Signal attenuation (low amplitude) in GPR radagram was visualized after applying Gain Function with 5 db/m different exponents growth function	108
Figure 3. 33	Hyperbola fitting in GPR signal image that generated the velocity and accurately gained accurate depth measurement	110
Figure 3. 34	Detail Description of GPR Signal Image Interpretation and Empirical Relationship Model	111
Figure 3. 35	The Agilent Vector Network Analyzer (PNA) E8562B	115
Figure 3. 36	The measurement of dielectric permittivity using the high-temperature dielectric probe method	115
Figure 3. 37	Calibration kits for Short-Open-Match method	117
Figure 3. 38	Calibration measurement for reference liquid (water) for VNA	117
Figure 3. 39	VNA Calibration Process by Short-Open-Match method : (a) “Open” in air, (b) Shorting termination (shorting block to the block) and (c) reference liquid (water)	119
Figure 3. 40	Measurement in-situ for the validation of empirical relationship modeling: a) Site preparation, followed by b) GPR measurement	120
Figure 3. 41	Planting of PVC pipes at a depth of 0.5m for diesel fuel spill channels.	120
Figure 3. 42	Automated classification mapping process for GPR signal's image classification	121
Figure 3. 42	Optimal Hyperlane using PolyKernel Function	122
Figure 4. 1	Comparison of amplitude GPR signal noise with filtered signal for contaminated Terap Red soil	127
Figure 4. 2	Noise level plot of GPR signal processed for both soil with different conditions.	128
Figure 4. 3	The variation of reflections of the processed GPR data for diesel migration based on temporal difference: 1) Red colour arrow representing the pipeline location and 2) Yellow colour arrow representing the diesel migration on contaminated Terap Red soil	131
Figure 4. 4	Particle size distribution curve for the Terap Red Soil and Sand	135

Figure 4. 5	The variation of reflections of the processed GPR data for diesel migration based on temporal difference: 1) Red colour arrow representing the pipeline location and 2) Yellow colour arrow representing the diesel migration and water fragmentation on contaminated sandy	137
Figure 4. 6	Specific geometric configurations for Clinofom classification, modified by Mitchum et al. (1977)	138
Figure 4. 7	The potential of velocity performance with changes in dielectric permittivity from GPR data reflection for contaminated Terap Red soil	142
Figure 4. 8	The potential of velocity performance with changes in dielectric permittivity from GPR data reflection for contaminated sandy soil	145
Figure 4. 9	The relationship and correlation between dielectric permittivity calculated by the GPR data and soil moisture content for contaminated Terap Red soil	148
Figure 4. 10	The schematic presentation of the effects of soil moisture content on the identification of permittivity constant of contaminated Terap Red Soil	149
Figure 4. 11	The relationship and correlation between dielectric permittivity calculated by the GPR data and soil moisture content for contaminated sandy soil	151
Figure 4. 12	The schematic presentation of the effects of soil moisture on the identification of permittivity constant of contaminated sandy soil	153
Figure 4. 13	Line of a fit plot of the empirical relationship model for Contaminated Terap Red soil	157
Figure 4. 14	Comparison chart for values between $\epsilon_r$ predicted and $\epsilon_r$ measured for all types of empirical relationship models influenced by the percentage of moisture content in contaminated Terap Red soil	160
Figure 4. 15	The residual plot of $\epsilon_r$ predicted value obtained from empirical relationship model compared to $\epsilon_{r(m)}$ measured value from GPR measurement for contaminated Terap Red soil	161
Figure 4. 16	Frequent quantitative estimates of $\epsilon_r$ predicted value obtained from empirical relationship model compared to $\epsilon_{r(m)}$ measured value from GPR measurement for contaminated Terap Red soil	161
Figure 4. 17	Boxplot of comparison chart for RMSE <sub>predicted</sub> values for all empirical relationship models for contaminated Terap Red soil	162

Figure 4. 18	Line of a fit plot of the empirical relationship model for contaminated sandy soil	164
Figure 4. 19	Comparison chart for values between $\epsilon_r$ predicted and $\epsilon_r$ measured for all types of empirical relationship models influenced by the percentage of moisture content in contaminated sandy soil	168
Figure 4. 20	The residual plot of $\epsilon_r$ predicted value obtained from empirical relationship model compared to $\epsilon_{r(m)}$ measured value from GPR measurement for contaminated sandy soil	169
Figure 4. 21	Frequent quantitative estimates of $\epsilon_r$ predicted value obtained from empirical relationship model compared to $\epsilon_{r(m)}$ measured value from GPR measurement for contaminated sandy soil	169
Figure 4. 22	Boxplot of comparison chart for RMSE predicted values for all empirical relationship models: (i) blue: third-order polynomial, (ii) orange: second-order polynomial, (iii) grey: logarithmic, and (iv) yellow: simple linear on contaminated sandy	170
Figure 4. 23	Frequency of $\epsilon_r$ predicted value obtained from empirical relationship model compared to $\epsilon_{r(m)}$ measured value from GPR measurement for contaminated Terap Red soil	174
Figure 4. 24	Comparison boxplot for values between $\epsilon_r$ predicted and $\epsilon_r$ measured for all empirical relationship models for contaminated Terap Red soil	176
Figure 4. 25	Series dielectric permittivity value for contaminated Terap Red soil from calibrated VNA measurement	177
Figure 4. 26	Comparison chart for values $\epsilon_r$ predicted and $\epsilon_r$ measured for all types of empirical relationship models influenced by the percentage of moisture content between VNA value for Terap Red soil	179
Figure 4. 27	Frequency of $\epsilon_r$ predicted value obtained from empirical relationship model compared to $\epsilon_{r(m)}$ measured value from GPR measurement for contaminated sandy soil	182
Figure 4. 28	Boxplot of comparison for values between $\epsilon_r$ predicted and $\epsilon_r$ measured values for all empirical relationship models for contaminated sandy soil	183
Figure 4. 29	Value of dielectric permittivity from a series of measurements for contaminated sandy soil using a VNA calibrated to a specified frequency (200Mhz to 10 GHz)	185
Figure 4. 30	Comparison chart for values between $\epsilon_r$ predicted and $\epsilon_r$ measured for all types of empirical relationship models with calibrated VNA in contaminated sandy soil	186

Figure 4. 31	Classifier Segmentation of contaminated Terap Red soil in GPR signal image for the training dataset	188
Figure 4. 32	Classifier Segmentation of contaminated sandy soil in GPR signal image for the training dataset	188
Figure 4. 33	Accuracy of contaminated soil classification mapping model between SVM and LR model for (a) contaminated Terap Red soil, (b) contaminated sandy soil	191
Figure 4. 34	Scatter plots of contaminated soil in different classification models for Terap Red soil: (a) the Support Vector Machine (SVM); (b) the Logistic Regression (LR)	192
Figure 4. 35	Scatter plots of contaminated soil in different classification models for sandy soil: (a) the Support Vector Machine (SVM); (b) the Logistic Regression (LR)	193
Figure 4. 36	Visualization for contaminated Terap Red soil using SVM: (a) classification visualization with support vectors (b) classification visualization boundaries only	194
Figure 4. 37	Visualization for contaminated sandy soil using SVM: (a) classification visualization with support vectors (b) classification visualization boundaries only	194
Figure 4. 38	The relationship and correlation between dielectric permittivity calculated by the in-situ GPR data and soil moisture content for contaminated Terap Red soil	195
Figure 4. 39	Classifier Segmentation of contaminated Terap Red soil in GPR signal image for the training dataset	196
Figure 4. 40	Scatter plots of contaminated soil in different classification models for in-situ contaminated Terap Red soil for the SVM Classifier	197
Figure 4. 41	Visualization for in-situ contaminated Terap Red soil using SVM: (a) classification visualization with support vectors (b) classification visualization boundaries only	197

## LIST OF ABBREVIATIONS

AGC	-	Automatic Gain Control
AI	-	Artificial Intelligence
ANOVA	-	Analysis of Variance
ANN	-	Artificial Neural Network
ASTM	-	American Society for Testing and Materials
BS	-	British Standard
CO <sub>2</sub>	-	Carbon Dioxide
CH <sub>4</sub>	-	Methane
CO	-	Common-offset
CMP	-	Common Mid-Point
CRIM	-	Complex Refractive Index Model
DEPs	-	Diesel Exhaust Particles
DNAPLs	-	Dense Non-Aqueous Phase Liquids
ERT	-	Electrical Resistivity Tomography
EM	-	Electromagnetic
GWC	-	Gravimetric Water Content
GPR	-	Ground Penetrating Radar
IPCC	-	Intergovernmental Panel on Climate Change
IARC	-	International Agency for Research on Cancer
LFL	-	Lower Flammability Limit
LNAPL	-	Light Non-Aqueous Phase Liquid
LR	-	Logistic Regression
MAE	-	Mean Absolute Error
NAPL	-	Non-Aqueous Phase Liquids
N <sub>2</sub> O	-	Nitrous Oxide
NRSME	-	Normalise Root Mean Square Error
PM <sub>2.5</sub>	-	Particulate Matter 2.5
PCB	-	Polychlorinated Biphenyl Oil
PVC	-	Polyvinyl Chloride
RMSN	-	Root Mean Square Noise

RMS velocity	-	Root Mean Square Velocity
SARS-CoV-2	-	Severe Acute Respiratory Syndrome Coronavirus 2
SMO	-	Sequential Minimal Optimization
SNR	-	Signal-to-noise Ratio
SVM	-	Support Vector Machine
TDR	-	Time Domain Reflectometry
USDA	-	United States Department Of Agriculture
VOCs	-	Volatile Organic Compounds
VNA	-	Vector Network Analyzer
WARR	-	Wide-Angle Reflection And Refraction



## LIST OF SYMBOLS

$w$	-	Moisture Content Expressed as A Percentage (%)
$m_2$	-	Weight of the container + weight of moist soil or wet soil (kg)
$m_3$	-	Weight of the container + weight of the dry soil (kg)
$m_1$	-	Weight of the container (kg)
$W_t$	-	Wet weight of contaminated soil (kg)
$W_d$	-	Dry weight of contaminated soil (kg)
$m$	-	Oil residual after drying
$n$	-	Oil content before drying
$I_p$	-	Plasticity index,
$W_L$	-	Result of liquid limit, and
$W_p$	-	Result plastic limit
$\rho_s$	-	Particle density ( $\text{g}/\text{cm}^3$ )
$\rho_b$	-	Bulk density.
$M_s$	-	Oven-dried soil (mass of only soil) in gram (g)
$m_{p1}$	-	Mass of pycnometer and cap assembly (in gram),
$m_{p2}$	-	Mass of pycnometer, cap and soil (in gram),
$m_{p3}$	-	Pycnometer, cap, soil and water (in gram)
$m_{p4}$	-	Mass of pycnometer, cap and water (in gram).
$V_s$	-	Total volume in $\text{cm}^3$ .
$V_l$	-	Volume of liquid
$V_g$	-	Volume of gas.
$\phi$	-	Porosity of the soil
$v$	-	Velocity of GPR electromagnetic wave ( $\text{m ns}^{-1}$ ),
$c$	-	Speed of light in a vacuum ( $0.3 \text{ m/ns}$ )
$\varepsilon$	-	Dielectric permittivity
$\frac{\delta}{\omega\varepsilon}$	-	Attenuation factor, $\omega = 2\pi f$ in $\text{rad s}^{-1}$

$\mu$	-	Magnetic permeability
$v_{LNAPL-soil}$	-	Velocity of LNAPL contaminated
$d$	-	Depth
$f_s$	-	Sampling frequency step
$T$	-	Required unambiguous time duration
$y$	-	Distance (m) in a vertical line,
$x$	-	Horizontal line's distance (m).
$A$	-	Amplitude,
$k$	-	Wavenumber (in <i>radian/m</i> ) which comes by $k = 2\pi/\lambda$
$\omega$	-	Angular frequency in ( <i>radians/s</i> )
$\emptyset$	-	Phase constant.
$\epsilon_{sw}$	-	Dielectric permittivity of the only soil-water mixture,
$\epsilon_s$	-	Dielectric permittivity of soil particles,
$\epsilon_w$	-	Dielectric permittivity of water,
$\epsilon_a$	-	Dielectric permittivity of air,
$\epsilon_{sNAPL}$	-	Dielectric permittivity of the soil-NAPL mixture,
$\epsilon_{sw-NAPL}$	-	Dielectric permittivity of the soil-water-NAPL mixture
$S$	-	Degree of saturation, $\phi$ is the porosity of the soil
$R$	-	Correlation coefficient
$r^2$	-	Variance (correlation coefficient),
$Y$	-	Dependent variable from regression and
$Y_p$	-	A predicted value of Y from linear regression and
$\bar{Y}$	-	Dependent variable's mean
$t$	-	T-test value,
$\bar{x}_1$	-	Score mean
$\sigma_1^2$	-	Variance of group
$f(k)$	-	Signal or amplitude of the raw data containing noise at a given scale level k to N, N is the length of the electromagnetic signal
$r(k)I$	-	De-noised signal or amplitude
$x_i, x_j$	-	Vectors in the input space

- $x_i^T x_j$  - A scalar product of the vectors in the input,
- $\alpha$  - Inner product based on some mapping in a feature space
- $\gamma$  - Parameter that is inversely proportional to the Gaussian kernel's width.

## LIST OF APPENDICES

<b>APPENDIX</b>	<b>TITLE</b>	<b>PAGE</b>
Appendix A	Raw Data of Terap Red from Moisture Content Test and GPR Signal Image	244
Appendix B	Dielectric Permittivity Predict Value for All Type Regression on Terap Red Soil	245
Appendix C	Raw Data Sandy Soil from Moisture Content Test and GPR Signal Image	246
Appendix D	Dielectric Permittivity Predict Value for All Type Regression on Sandy Soil	247
Appendix E	Table Of Significant Values for T-Distribution (Chua, 2006)	248
Appendix F	Table Of Significant Values for F-Distribution (Chua, 2006)	249
Appendix G	Sieve Analysis Test on Terap Red Soil and Sandy Soil	251
Appendix H	Atterberg Limit Test on Terap Red Soil and Sandy Soil for both Clean and Contaminated	253
Appendix I	Particle Density Test on Terap Red Soil and Sandy Soil	257
Appendix J	VNA Probe Test Calibration (Water)	258
Appendix K	Training Dataset Terap Red	259
Appendix L	Training Dataset for Sandy Soil	265
Appendix M	Observation dan Predict Dielectric Permittivity Value with Moisture Content	272
Appendix N	Training Dataset for In-Situ Contaminated Terap Red soil	273

# CHAPTER 1

## INTRODUCTION

### 1.1 Research Background

Diesel fuel which is part of hydrocarbon, is a distilled fuel oil used in motor vehicles and electricity generation derived from crude oil and biomass composites (Gad, 2014; Latif et al., 2021). Diesel fuel contains sulfur, which can induce carcinogenic air pollution emissions in humans, according to the International Agency for Research on Cancer (IARC), obtained by Gad (2014) and Mueller et al. (2021). Carcinogenic substances are chemicals or chemical mixtures that have the potential to cause cancer in humans (Hentz, 2010; Mueller et al., 2021). Several studies, including Mustafa et al. (2020) and Mueller et al. (2021), have associated diesel exhaust particles (DEPs), a key element of atmospheric particulate matter  $<2.5\mu\text{m}$  (PM<sub>2.5</sub>), as a mechanism of severe acute respiratory syndrome coronavirus 2 (SARS-CoV-2) risk, which tends to increase inflammation and severe lung damage as shown in Figure 1.1. In summary, contamination of diesel fine Particle Matter 2.5 (dPM<sub>2.5</sub>) provides an appropriate medium for keeping” and carrying” the SARS-CoV-2 during respiratory air transportation, as illustrated in Figure 1.1. Figure 1.1 also depicts multiple routes of virus replication into the human pulmonary system, such as type II pneumocytes expressing Angiotensin-converting enzyme 2 (ACE2) receptors, which allow SARS-CoV-2 with dimensions of 70–90 nm to enter and spread over host cells

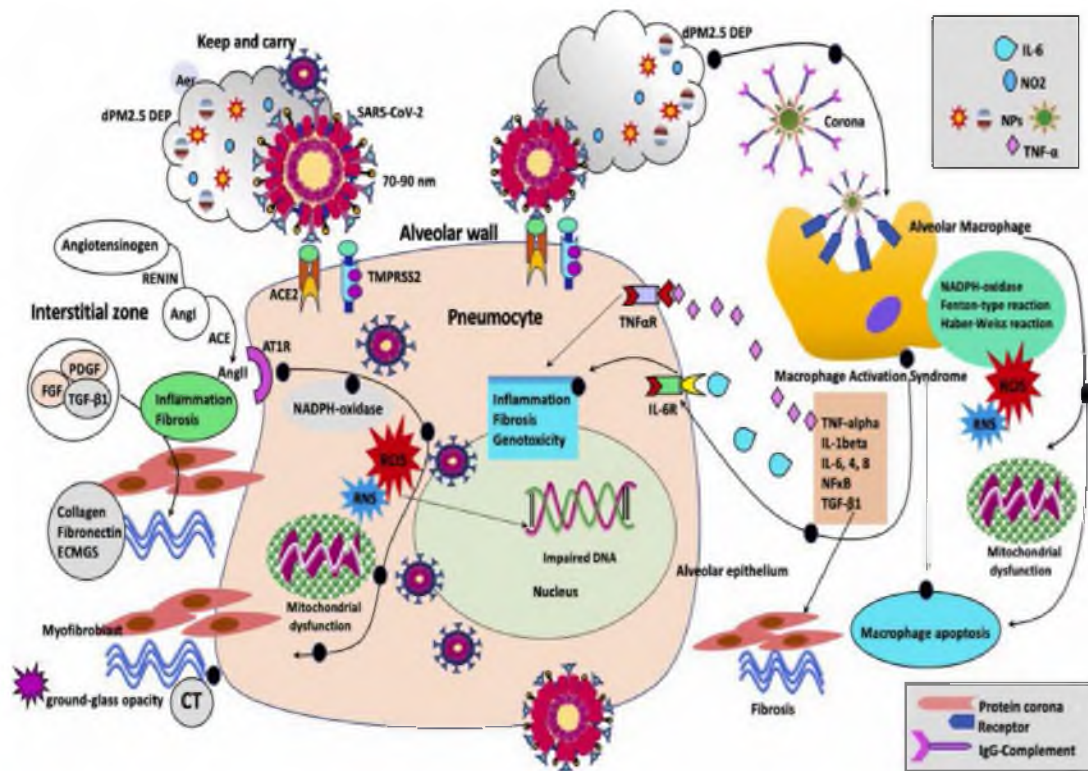


Figure 1.1 The molecular mechanism of typical pulmonary lesions induced by DEP and SARS-CoV-2 exposure in the environment, adopted from (Mustafa et al., 2020)

In the energy industry, the emission factor from diesel, particularly Carbon dioxide (CO<sub>2</sub>) emissions, which can produce greenhouse effects, is also relatively high, as reported by Intergovernmental Panel on Climate Change (IPCC) in Table 1.1, as stated by Latif et al. (2021). Consequently, the use of diesel for power energy in Malaysia began to decline in 2014, with the potential substitute of renewable energy such as solar energy, as illustrated in Figure 1.2 reported by Latif et al. (2021).

Meanwhile, diesel as a soil contaminant can be toxic to plants and soil microorganisms and contaminate groundwater. Diesel fuel can reduce the bioconcentration index of nitrogen, phosphorus, calcium, and potassium as in corn, as well as negatively impact the physical properties of the soil. Influence on the physical properties of soils, such as water retention and unsaturated hydraulic conductivity, caused by diesel contamination depends on the characteristics of the soil contaminated. In addition to the effects on soil properties and water, the retention of diesel and diesel vapor in the soil can induce flames and explosions when mixed with air since diesel fuel is classified as a flammable liquid with a flame point below 60°C (Karim, 1980).

Table 1.1 Emission factor for stationary combustion in the energy sector based on kg of greenhouse gas per TJ on a Net Calorie Basis, according to the IPCC report (Latif et al., 2021)

Fuel Type	CO <sub>2</sub> (kg/TJ)	CH <sub>4</sub> (kg/TJ)	N <sub>2</sub> O (kg/TJ)
Natural gas	56,100	1	0.1
Residual fuel oil	77,400	3	0.6
Diesel fuel	74,100	3	0.6
Other bituminous coal	94,600	1	1.5
Sub-bituminous coal	96,100	1	1.5
Industrial waste (Biomass)	143,000	30	4
Other biogas	54,600	1	0.1

\*CH<sub>4</sub>: Methane, N<sub>2</sub>O: Nitrous oxide

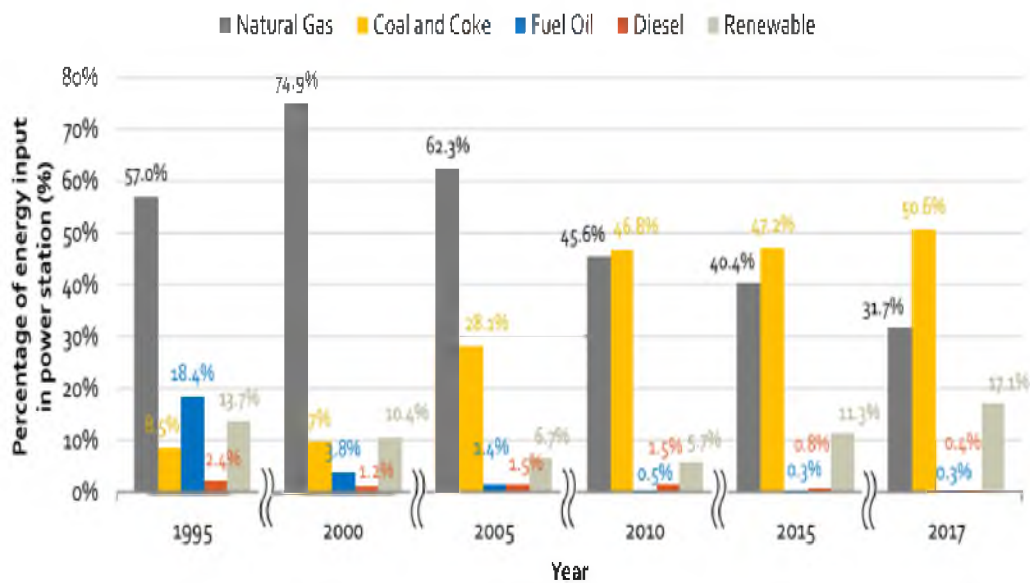


Figure 1.2 Percentage of energy source inputs used in power plants (Latif et al., 2021)

Since diesel retention in this soil depends on soil properties such as particle size and porosity, measurements for environmental risk assessment and remediation are essential, and many studies have been conducted (Kia & Abdul, 1990). With this awareness, fuel-related safety laws have been enforced, such as in Malaysia, governed by Act 302 - Petroleum (Safety Measures) Act 1984. Since 1980, various approaches to diesel contamination detection studies in soil, including laboratory and field studies,

have been introduced to satisfy legal and safety requirements on health and the environment. Some common methods that have been introduced include geotechnical studies such as moisture content test, liquid limit test, direct shear test, and grain size distribution to assess the retention effects of diesel (Hernández-Mendoza, García Ramírez, & Chávez Alegría, 2021). In addition, the geophysical technique is frequently used to map diesel-contaminated soils in situ. Geophysical methods include neutron probes and Time Domain Reflectometry (TDR), Electrical Resistivity Tomography (ERT), and Ground Penetrating Radar (GPR).

The neutron probe and TDR methods are ground-based intrusive methods suitable for high spatial diversity of soil moisture and provide point measurements with limited sampling (Charlton, 2008). In contrast, ERT for bottom surface structure imaging is based on direct conductivity measurement on a shallow surface using electrodes with time-lapse photographic imaging (Glaser et al., 2012; Meyer et al., 2013). GPR is a non-destructive geophysical method that measures changes in the electrical properties of soil to provide a high-resolution picture of subsurface variations (Darayan et al., 1998; Lu et al., 2017).

GPR could identify bulk dielectric contrasts in varying volumetric mixtures of soil, air, water, and hydrocarbons (Glaser et al., 2012). It is based on a pulse radar system that transmits short electromagnetic pulses into a medium where some energy is reflected while the remaining travels forward (Porubiaková & Komačka, 2015). This radar's travel function is determined by electromagnetic properties such as dielectric permittivity ( $\epsilon$ ), magnetic permeability ( $\mu$ ), and electrical conductivity ( $\sigma$ ) (Martinez & Byrnes, 2001). The more significant the dielectric permittivity difference between the materials on the bottom surface, the higher the amplitude of reflection produced, as calculated by the amplitude reflection coefficient ( $R$ ) (Glaser et al., 2012).

Dielectric permittivity is a complex function of the capacity to store energy when an electric field alternates in free space (Klotzsche et al., 2018; Paula Castillo, 2015). Dielectric permittivity can also be defined as the ratio of an electric field's strength in a vacuum to that encountered in a material with the same charge distribution (Palneedi et al., 2021; Xu, 2016; Yalcin et al., 2015). The dielectric permittivity varies



with the temperature and frequency of the electric field, depending on the material structure, composition, and lattice flexibility (Jiang et al., 2018; Palneedi et al., 2021). The dielectric permittivity can be measured using Vector Network Analyzer (VNA) in laboratory (Yalcin et al., 2015; Jafery et al., 2018; Szyplowska et al., 2018), parallel plate capacitors (Palneedi et al., 2021; Taflove & Hagness, 2005), velocity equations (Weihnacht & Boerner, 2014; Wijewardana et al., 2017; Liu et al., 2020), empirical equations (Topp et al., 1980; Curtis, 2001; Park et al., 2017; Tempke et al., 2018) and volumetric mixing formulas (Bano, 2004; Iravani et al., 2020; Roth et al., 1990; Wharton et al., 1980). Dielectric permittivity is also used in modeling the image classification of GPR signals for GPR data interpretation via artificial intelligence (AI) (Cabrera, 2015; Travassos, Avila, et al., 2021) and machine learning (Millington & Cassidy, 2010; Muniappan & Balasubramani, 2011; El-Mahallawy & Hashim, 2013; Economou et al., 2017; Giannopoulos, 2005; Liu et al., 2020; Travassos et al., 2021).

The machine learning algorithm is a subset of Artificial Intelligence (AI) based on statistical learning theory that enables automatic classification and data analysis from experience (Muniappan & Balasubramani, 2011). Support Vector Machine (SVM) is a widely used machine learning algorithm for mapping the locality of GPR image hyperbola patterns that employs the principle of supervised learning for classification and regression analysis (Pasolli et al., 2008; Muniappan & Balasubramani, 2011; Travassos et al., 2018; Zadhoush et al., 2021). SVM classifies binary data by defining a divider hyperplane in a high-dimensional feature space and obtaining the maximum margin between classes from training data via GPR data segmentation (Muniappan & Balasubramani, 2011; Nishimoto et al., 2006). In classifying GPR data, according to Muniappan & Balasubramani (2011) and Pasolli et al. (2008), SVM can achieve higher accuracy and is very useful in reducing noise in GPR signal images. As an outcome, SVM has been used in this study to improve the accuracy of the interpretation of diesel-contaminated soil from GPR data segmentation.

## 1.2 Problem Statement

Terap Red has clayey over clayey-skeletal, kaolinite, isohyperthermic, and typical hapludults according to the USDA Soil Taxonomy as published in Malaysia Common Soil of Peninsular Malaysia by Malaysia Department of Agriculture in 2018 and Malaysia Soil Taxonomy by Paramanathan (2020). Terap Red soil has been classified as a type of laterite-reworked soil based on the characteristics of clay and other mixtures (DOA, 2018) Terap red soil is a type of soil found throughout Peninsular Malaysia, accounting for nearly 40% of the north part of the peninsular (DOA, 2018). Due to its high water retention properties, this lateritic soil is typically used as a soil liner to retain wastewater from solid waste and petroleum substances in landfill areas in Malaysia (Syafalni et al., 2015) and India (Thankam et al., 2017) and many more. However, if the soil is in an agricultural or residential area, sudden contamination, especially from diesel machinery or vehicles or the deliberate disposal of diesel waste, is likely to pose a significant problem.

According to Hewelke et al. (2018), 60 % of soil contamination in the European Union is caused by fuel minerals and heavy metals. In Malaysia, contamination from diesel was reported in the Sungai Langat, Selangor area by Mohamed (2022) from Kosmo on 27 July 2019 and the industrial area of Tanjung Kidurong, Sarawak by Department of Environment Malaysia (DOE) on 29 October 2020. Apart from harming the environment, the retention of diesel fuel in soils higher than water (Kia & Abdul, 1990) and the evaporation of diesel fuel are the factors that contribute to changes in the physical properties of the contaminated soil, particularly lateritic soils. For instance, as per a study by Sharma (2014), (Hewelke et al. (2018), and Hernández-Mendoza et al. (2021), diesel's presence in sandy soils has decreased the optimal moisture content of the soil and increased its plasticity and friction angle. However, the effect of diesel fuel in the soil will be different for each type of soil because of the unique characteristics of each soil.

Therefore, numerous studies, including the evaluation of GPR wave signal, have been conducted to evaluate the impact of diesel fuel on various types of soil. As an example, Daniels et al. (1995), Bano et al. (2009), Guo et al. (2012), and Mansi et

al. (2017) have successfully identified apparent GPR signal anomalies in sandy soils contaminated with diesel. Nevertheless the reflection of the GPR signal is dependent on the physical and electromagnetic properties of the soil particularly the dielectric permittivity as the diesel effect of the soil varies with soil type as mentioned by Mansi et al. (2017) and Shamir et al. (2018). Additionally, the dielectric permittivity of each soil influences the accuracy of the GPR's depth measurement and resolution. This is due to the close relationship between dielectric permittivity and velocity, which determines the depth and wavelength of the GPR (resolution).

Considering the importance of dielectric permittivity, several studies have been conducted to predict dielectric permittivity's, such as Topp's model (Topp et al., 1980) and the complex refractive index method (CRIM) model (Comegna et al., 2016). Both models are frequently employed in some GPR-based studies, but each has its limitations. Patriarca et al. (2013) revealed that Topp's model underestimates the turbulence of high-bound water, such as clay, while overestimating the turbulence of low-bound water, such as sand. While Steelman & Endres (2011) claimed that changes in the shape factor of soil texture in the CRIM model are difficult to determine, contributing to the low accuracy of dielectric permittivity prediction. As a result, it motivates establishing a new empirical relationship model for predicting the dielectric permittivity of contaminated Terap Red soils in GPR measurements. This model's establishment is also supported by Al-mattarneh et al. (2013), Rubin & Ho (2018), and Mironov et al. (2019), which explain that each dielectric prediction model is only adequate for specific soils

In addition, interpretation of the GPR signal is difficult since the amplitude of the GPR signal waveform varies depending on the dielectric permittivity. Its intrinsic image is exposed to and qualitatively constrained by noisy data or nonlinear interaction issues from other devices. This issue will complicate the mapping of the distribution of contaminated soil by diesel using GPR, owing to the uncertainty of changes in contaminated soil characteristics. As a result, many studies on the reliability of GPR signal image explanation through automatic classification mapping, such as SVM (Wu et al., 2008; Pasolli et al., 2009), have been conducted. Regrettably, the automatic classification mapping method used by researchers such as Pasolli et al. (2008) is for

objects permanently buried beneath the subsurface. Consequently, studies must be conducted to classify GPR signals using machine learning techniques such as SVM for diesel contamination, a movable material that induces uncertainty in soil.

### **1.3 Objectives**

The study aims to assess the feasibility of using high-frequency GPR to characterize and retrieve the dielectric permittivity and determine the location of contaminated Terap Red soils triggered by diesel in the subsurface. In addition, studies on sandy soils, which some researchers commonly use, are also conducted as a comparison for optimized findings. Specific objectives for this thesis are:

- i. To investigate the effect of diesel presence on soil properties and retrieve the dielectric permittivity of diesel-contamination in Terap Red soil from wave velocity in GPR.
- ii. To establish an empirical relationship model between dielectric permittivity and variations in soil moisture content of diesel-contamination in Terap Red soil.
- iii. To assess and validate the accuracy of the proposed empirical relationship for the prediction of dielectric permittivity of diesel-contamination in Terap Red soil.
- iv. To delineate and improve the mapping of diesel-contaminated soil plume output using a Support Vector Machine classifier based on GPR signal images corrected with predicted dielectric permittivity.

### **1.4 Significance of the Study**

Terap Red soil is classified as a lateritic soil with high nutrients suitable for agricultural purposes, landfill soil liner and widespread distribution throughout Peninsular Malaysia's northwestern region. The presence of diesel spills from agricultural machinery or power generators will modify the soil nutrients, so this

contaminated soil detection study is required to utilize GPR as a non-invasive and non-destructive method for the large-scale identification of diesel-contaminated soil. Since GPR is dielectric dependent, and the existing dielectric permittivity calculation study is limited to specific soils, it is essential that a dielectric calculation study for Terap Red soils is performed and compared to sandy soils.

Furthermore, the depth accuracy and resolution of GPR measurements dependent on velocity value can be improved with the prediction of the soil dielectric. Besides that, the GPR signal image is difficult to interpret due to dielectric changes caused by the presence of diesel in the soil. As a result, through automatic classification mapping, the image assessment of the GPR signal can be improved.

## **1.5 Scope and Limitation**

This study focused solely on detecting diesel contamination in Tanah Terap obtained from agricultural areas in the state of Perlis. Diesel detection was performed on a large-scale tank simulation constructed of concrete with dimensions of 1.9m x 2.5m x 1.5m and a thickness of 5cm. The use of concrete blocks is based on high conductivity material criteria (Wu et al., 2013), which control the propagation of electromagnetic (EM) waves. It can distinguish the area between simulation sites. This model applies to field and laboratory measurements to determine the parameters for constructing empirical relationships for dielectric prediction and evaluating diesel effects in the soil. Field measurements include two procedures: high-frequency GPR measurement at 800MHz, which produces high-resolution GPR images, and soil moisture probe testing. All geotechnical laboratory tests are based on British Standard (BS) to determine the properties of Terap Red and sandy soils. Furthermore, the validation of dielectric permittivity predictions is limited to comparing existing models commonly used in validation studies and in-situ testing of the VNA. Automated classification mapping for GPR signal images only using SVM classifier with comparison using Logistic Regression (LR) in WEKA software

## 1.6 Thesis Outline

This thesis is divided into five chapters. The first chapter discusses the study's background, problem statement, objectives, the significance of the study, the scope of the study, and research contribution.

Chapter 2 highlights the definition of contaminated soil; the concept of GPR measurement includes dielectric permittivity parameters and GPR data processing and descriptions of geotechnical tests and statistical tests for empirical relationships. In addition, the effect of the presence of diesel on soil properties is discussed. This chapter also presents some techniques used to detect contaminated soils, including existing dielectric determination studies.

Chapter 3 describes the detailed methodology, including selecting materials for the construction of soil contamination simulation sites and soil samples suitable for the study. This chapter also includes the method of data collection, GPR data processing, empirical relationship construction, and mapping of contaminated soil classification models.

In Chapter 4, the study's findings and statistical analysis, along with a discussion of the research methodology. In this chapter, each study result, analysis, and discussion are described based on the study's objectives. Next, this chapter describes GPR signal interpretation analysis results in conjunction with geotechnical results. Furthermore, the results of establishing an empirical relationship model between dielectric permittivity and soil content and statistical results and an accuracy assessment, followed by verification results. This chapter also includes the results and analysis of contaminated soil classification mapping for GPR data using SVM and LR classifiers.

Finally, chapter 5 concludes the study's findings, referring to the study's objectives, study contribution, limitations, and recommendations for future research.

## REFERENCES

- Abbas, M., Jardani, A., Machour, N., & Dupont, J. P. (2018). Geophysical and geochemical characterisation of a site impacted by hydrocarbon contamination undergoing biodegradation. *Near Surface Geophysics*, 16(2), 176–192. <https://doi.org/10.3997/1873-0604.2017061>
- Abdelgwad, A. H., & Said, T. M. (2016). Measured dielectric permittivity of contaminated sandy soil at microwave frequency. *Journal of Microwaves, Optoelectronics and Electromagnetic Applications*, 15(2), 115–122. <https://doi.org/10.1590/2179-10742016v15i2591>
- Adebayo Bayo, O. M. O. (2015). *Evaluation of Suitability of Selected Dredged Sand and Sludge for Engineering Application. March 2013.*
- Ahmadian, N., Hasan, S., & Calla, O. P. N. (2013). Permittivity and backscattering coefficient of diesel oil-contaminated soil at C Band (5.3 GHz). *International Journal of Microwave Science and Technology*, 2013. <https://doi.org/10.1155/2013/950862>
- Ai, Q., Liu, Q., Meng, W., & Xie, S. Q. (2018). Neuromuscular Signal Acquisition and Processing. In *Advanced Rehabilitative Technology*. <https://doi.org/10.1016/b978-0-12-814597-5.00003-5>
- Al-mattarneh, H., Dahim, M., & Malkawi, A. (2013). Dielectric Measurement for Characterization of Sandy Soil Contaminated by Diesel. *29th Annual International Conference on Soils, Sediments, Water and Energy, January 2016.*
- Alesse, B., Orlando, L., & Palladini, L. (2019). Non-invasive lab test in the monitoring of vadose zone contaminated by light non-aqueous phase liquid. *Geophysical Prospecting*, 67(8), 2161–2175. <https://doi.org/10.1111/1365-2478.12809>
- Alhassan, H. M., & Fagge, S. A. (2013). Effects of crude oil, low point pour fuel oil and vacuum gas oil contamination on the geotechnical properties of sand , clay and laterite soils. *International Journal of Engineering Research and Applications*, 3(1), 1947–1954.

- Alhumimidi, M. S., Harbi, H. M., Alfarhan, M. S., Abdelrahman, K., & Aiken, C. L. V. (2017). *Imaging fracture distributions of the Al-Khuff Formation outcrops using GPR and ERT geophysical techniques , Al-Qassim area , Saudi Arabia.* <https://doi.org/10.1007/s12517-017-3059-0>
- Amador-Muñoz, O., Martínez-Domínguez, Y. M., Gómez-Arroyo, S., & Peralta, O. (2020). Current situation of polycyclic aromatic hydrocarbons (PAH) in PM2.5 in a receptor site in Mexico City and estimation of carcinogenic PAH by combining non-real-time and real-time measurement techniques. *Science of the Total Environment*, 703, 134526. <https://doi.org/10.1016/j.scitotenv.2019.134526>
- Amran, T. S. T., Ismail, M. P., Ahmad, M. R., Amin, M. S. M., Ismail, M. A., Sani, S., Masenwat, N. A., & Basri, N. S. M. (2018). Monitoring underground water leakage pattern by ground penetrating radar (GPR) using 800 MHz antenna frequency. *IOP Conference Series: Materials Science and Engineering*, 298(1). <https://doi.org/10.1088/1757-899X/298/1/012002>
- Annan, A. P. (2003). Ground Penetrating Radar Principles, Procedure & Applications. In *Ground Penetrating Radar Theory and Applications: Vol. Ground Pen.* <https://doi.org/10.1016/B978-0-444-53348-7.00016-8>
- Arjoon, K., & Speight, J. G. (2020). Chemical and Physical Analysis of a Petroleum Hydrocarbon Contamination on a Soil Sample to Determine Its Natural Degradation Feasibility. *Inventions*, 1–10. <https://doi.org/10.3390/inventions5030043>
- Arnell, D. (2010). Mechanisms and laws of friction and wear. *Tribology and Dynamics of Engine and Powertrain: Fundamentals, Applications and Future Trends*, 41–72. <https://doi.org/10.1533/9781845699932.1.41>
- Arshad, M. A. C., Lowery, B., & Grossman, B. (2015). Physical tests for monitoring soil quality. *Methods for Assessing Soil Quality*, 123–141. <https://doi.org/10.2136/sssaspepub49.c7>
- Attom, M., Hawileh, R., & Naser, M. (2013). Investigation on concrete compressive strength mixed with sand contaminated by crude oil products. *Construction and Building Materials*, 47, 99–103. <https://doi.org/10.1016/j.conbuildmat.2013.04.042>



- Azimi, R., Vaezihir, A., Lenhard, R. J., & Majid Hassanizadeh, S. (2020). Evaluation of LNAPL behavior in water table inter-fluctuate zone under groundwater drawdown condition. *Water (Switzerland)*, *12*(9). <https://doi.org/10.3390/W12092337>
- Baili, J., Lahouar, S., Hergli, M., Al-Qadi, I. L., & Besbes, K. (2009). GPR signal denoising by discrete wavelet transform. *NDT and E International*, *42*(8), 696–703. <https://doi.org/10.1016/j.ndteint.2009.06.003>
- Balouet, J. C., Oudijk, G., Petrisor, I., & Morrison, R. D. (2007). Emerging forensic techniques. *Introduction to Environmental Forensics*, 671–731. <https://doi.org/10.1016/B978-012369522-2/50016-6>
- Bano, M. (2004). Modelling of GPR waves for lossy media obeying a complex power law of frequency for dielectric permittivity. *Geophysical Prospecting*, *52*(1), 11–26. <https://doi.org/10.1046/j.1365-2478.2004.00397.x>
- Bano, M., Loeffler, O., & Girard, J. F. (2009). Ground penetrating radar imaging and time-domain modelling of the infiltration of diesel fuel in a sandbox experiment. *Comptes Rendus - Geoscience*, *341*(10–11), 846–858. <https://doi.org/10.1016/j.crte.2009.08.002>
- Barrio-Parra, F., Izquierdo-Díaz, M., Díaz-Curiel, J., & De Miguel, E. (2021). Field performance of the radon-deficit technique to detect and delineate a complex DNAPL accumulation in a multi-layer soil profile. *Environmental Pollution*, *269*, 116200. <https://doi.org/10.1016/j.envpol.2020.116200>
- Bello, Y. Idi. (2013). *Mapping and Modelling Petrphysical Biogenic Gas Concentration of Pontian Peatland, Southwest Malaysia with Ground Penetrating Radar*. PhD Thesis. Universiti Teknologi Malaysia.
- Benedetto, A., & Benedetto, F. (2014). Application Field-Specific Synthesizing of Sensing Technology: Civil Engineering Application of Ground-Penetrating Radar Sensing Technology. In *Comprehensive Materials Processing* (Vol. 13). Elsevier. <https://doi.org/10.1016/B978-0-08-096532-1.01315-7>
- Benedetto, A., & Pajewski, L. (2015). *Civil Engineering Applications of Ground Penetrating Radar*. Springer Nature Switzerland. <https://doi.org/10.1007/978-3-319-04813-0>
- Bertolla, L., Porsani, J. L., Soldovieri, F., & Catapano, I. (2014). GPR-4D monitoring a controlled LNAPL spill in a masonry tank at USP, Brazil. *Journal of Applied Geophysics*, *103*, 237–244. <https://doi.org/10.1016/j.jappgeo.2014.02.006>

- Bęś, A., Warmiński, K., & Adomas, B. (2019). Long-term responses of Scots pine (*Pinus sylvestris* L.) and European beech (*Fagus sylvatica* L.) to the contamination of light soils with diesel oil. *Environmental Science and Pollution Research*, 26(11), 10587–10608. <https://doi.org/10.1007/s11356-019-04328-6>
- Besha, A. T., Bekele, D. N., Naidu, R., & Chadalavada, S. (2018). Recent advances in surfactant-enhanced In-Situ Chemical Oxidation for the remediation of non-aqueous phase liquid contaminated soils and aquifers. *Environmental Technology and Innovation*, 9, 303–322. <https://doi.org/10.1016/j.eti.2017.08.004>
- Birken, R., Ave, H., Schirner, G., Ave, H., Wang, M., & Ave, H. (2012). VOTERS : Design of a Mobile Multi-Modal Multi-Sensor System. *SensorKDD Workshop 2012: Proceedings of the Sixth International Workshop on Knowledge Discovery from Sensor Data*, 8–15. <https://doi.org/https://doi.org/10.1145/2350182.2350183>
- Bockheim, J. G., & Hartemink, A. E. (2013). Distribution and classification of soils with clay-enriched horizons in the USA. *Geoderma*, 209–210, 153–160. <https://doi.org/10.1016/j.geoderma.2013.06.009>
- Bordón, P., Bonomo, N., & Martinelli, P. (2019). Automatic detection of pipe-flange reflections in GPR data sections using supervised learning. *Journal of Applied Geophysics*, 170. <https://doi.org/10.1016/j.jappgeo.2019.103856>
- Bortoni, S. F., Schlosser, R. T., & Barbosa, M. C. (2019). Numerical modeling of Multiphase Extraction (MPE) Aiming at LNAPL recovery in tropical soils. *Water (Switzerland)*, 11(11). <https://doi.org/10.3390/w11112248>
- Bostanudin, N. J. F. (2013). *Computational Methods for Processing Ground Penetrating Radar Data* (Issue May). Master Thesis. University of Portsmouth.
- Bouزيد, I., Pino Herrera, D., Dierick, M., Pechaud, Y., Langlois, V., Klein, P. Y., Albaric, J., & Fatin-Rouge, N. (2021). A new foam-based method for the (bio)degradation of hydrocarbons in contaminated vadose zone. *Journal of Hazardous Materials*, 401(July 2020), 123420. <https://doi.org/10.1016/j.jhazmat.2020.123420>
- Bradford, J. H., Babcock, E. L., Marshall, H. P., & Dickins, D. F. (2016). Targeted reflection-waveform inversion of experimental ground-penetrating radar data for quantification of oil spills under sea ice. *Geophysics*, 81(1), WA59–WA70. <https://doi.org/10.1190/GEO2015-0170.1>

- Brevik, E. C., Calzolari, C., Miller, B. A., Pereira, P., Kabala, C., Baumgarten, A., & Jordán, A. (2016). Soil mapping, classification, and pedologic modeling: History and future directions. *Geoderma*, 264, 256–274. <https://doi.org/10.1016/j.geoderma.2015.05.017>
- Brewster, M. L., & Annan, A. P. (1994). Ground-penetrating radar monitoring of a controlled DNAPL release: 200 MHz radar. *Geophysics*, 59(8), 1211–1221. <https://doi.org/10.1190/1.1443679>
- Bridge, J. S., Alexander, J., Collier, R. E. L., Gawthorpe, R. L., & Jarvis, J. (1995). Ground-penetrating radar and coring used to study the large-scale structure of point-bar deposits in three dimensions. *Sedimentology*, 42(6), 839–852. <https://doi.org/10.1111/j.1365-3091.1995.tb00413.x>
- Bristow, C. S., & C.S.Bristow, H. M. J. (2009). Ground Penetrating Radar in Sediments. In *Geological Society of London* (Vol. 211).
- British Standards Institution. (1990). Soils for civil engineering purposes. *Part 8, BS 1377-4:(1)*, 40. <https://doi.org/10.1353/lan.2016.0052>
- Brown, J., Nichols, J., Steinbronn, L., & Bradford, J. (2009). Improved GPR interpretation through resolution of lateral velocity heterogeneity : Example from an archaeological site investigation. *Journal of Applied Geophysics*, 68(1), 3–8. <https://doi.org/10.1016/j.jappgeo.2008.08.014>
- Bu, Q. T., Hu, G. W., Ye, Y. G., Liu, C. L., Li, C. F., Best, A. I., & Wang, J. S. (2017). The elastic wave velocity response of methane gas hydrate formation in vertical gas migration systems. *Journal of Geophysics and Engineering*, 14(3), 555–569. <https://doi.org/10.1088/1742-2140/aa6493>
- Burazer, M., & Burazer, N. (2017). Geophysical and geochemical investigation of hydrocarbon subsurface contamination. *15th International Conference on Environmental Science and Technology Rhodes, September*, 1–5.
- C S Bristow, H. M. J. (2009). *Ground Penetrating Radar in Sediments (Geological Society Special Publication) (No. 211)*.
- Cabrera, D. A. (2015). *Characterization of components of water supply systems from GPR images and tools of intelligent data analysis* (Issue December). PhD Thesis. Polytechnic University of Valencia.
- Carcione, J. M. (2007). Chapter 3 Isotropic anelastic media. *Handbook of Geophysical Exploration: Seismic Exploration*, 38(1986), 97–138. [https://doi.org/10.1016/S0950-1401\(07\)80008-5](https://doi.org/10.1016/S0950-1401(07)80008-5)

- Cassidy, N. J. (2007). Evaluating LNAPL contamination using GPR signal attenuation analysis and dielectric property measurements: Practical implications for hydrological studies. *Journal of Contaminant Hydrology*, 94(1–2), 49–75. <https://doi.org/10.1016/j.jconhyd.2007.05.002>
- Cassidy, N. J. (2008). GPR Attenuation and Scattering in a Mature Hydrocarbon Spill: A Modeling Study. *Vadose Zone Journal*, 7(1), 140–159. <https://doi.org/10.2136/vzj2006.0142>
- Cassidy, N. J. (2009). Ground penetrating radar data processing, modelling and analysis. In *Ground Penetrating Radar* (First Edit, pp. 141–176). Elsevier. <https://doi.org/10.1016/B978-0-444-53348-7.00005-3>
- Chala, A. T., Matula, S., Bářková, K., & Doležal, F. (2019). Evaluation of methods for water and non-volatile LNAPL content measurement in porous media. *Soil and Water Research*, 14(1), 47–56. <https://doi.org/10.17221/80/2018-SWR>
- Charles R. Fitts. (2017). Physical Properties. In *Groundwater Science (Second Edition)* (pp. 23–45). Elsevier Inc. <https://doi.org/10.1016/B978-0-12-384705-8.00002-9>
- Charlton, M. B. (2008). Principles of ground-penetrating radar for soil moisture assessment. *Journal of Hydrology*, June.
- Chern, S. G., Hu, R. F., Li, C. Y., Pei, K. C., & Lin, D. W. (2005). A research combines geo-technique test and a three dimensional image GPR inspection for rigid pavement pumping failure. *Journal of Marine Science and Technology*, 13(1), 11–19.
- Chua, Y. P. (2006). *Asas statistik penyelidikan* (Issue August). McGraw-Hill Education (Asia); 2nd edition (March 1, 2012).
- Ciampoli, L. B., Tosti, F., Economou, N., & Benedetto, F. (2019). Signal processing of GPR data for road surveys. *Geosciences (Switzerland)*, 9(2). <https://doi.org/10.3390/geosciences9020096>
- Comegna, A., Coppola, A., Dragonetti, G., & Sommella, A. (2013). Dielectric Response of a Variable Saturated Soil Contaminated by Non-Aqueous Phase Liquids (NAPLs). *Procedia Environmental Sciences*, 19, 701–710. <https://doi.org/10.1016/j.proenv.2013.06.079>

- Comegna, A., Coppola, A., Dragonetti, G., & Sommella, A. (2016). Estimating nonaqueous-phase liquid content in variably saturated soils using time domain reflectometry. *Vadose Zone Journal*, 15(5). <https://doi.org/10.2136/vzj2015.11.0145>
- Copeland, K. A. F. (1997). Applied Linear Statistical Models. In *Journal of Quality Technology* (Vol. 29, Issue 2). <https://doi.org/10.1080/00224065.1997.11979760>
- Cornforth, D., Jelinek, H. F., & Khandoker, A. H. (2018). ECG Time Series Variability Analysis: Engineering and Medicine. In *Taylor & Francis Group* (Vol. 7, Issue 2). CRC Press. [https://doi.org/DOI: 10.4324/9781315372921-3](https://doi.org/DOI:10.4324/9781315372921-3)
- Cui, F., Du, Y., Ni, J., Zhao, Z., & Peng, S. (2021). Effect of shallow-buried high-intensity mining on soil water content in ningtiaota minefield. *Water (Switzerland)*, 13(3), 1–14. <https://doi.org/10.3390/w13030361>
- Cunningham, C. (2000). Comparison of bioaugmentation and biostimulation in ex situ treatment of diesel contaminated soil. *Land Contamination & Reclamation*, 8(January). <https://doi.org/10.2462/09670513.575>
- Curtis, J. O. (2001). Moisture effects on the dielectric properties of soils. *IEEE Transactions on Geoscience and Remote Sensing*, 39(1), 125–128. <https://doi.org/10.1109/36.898673>
- D’Emilio, M., Macchiato, M., Ragosta, M., & Simoniello, T. (2012). A method for the integration of satellite vegetation activities observations and magnetic susceptibility measurements for monitoring heavy metals in soil. *Journal of Hazardous Materials*, 241–242, 118–126. <https://doi.org/10.1016/j.jhazmat.2012.09.021>
- Dagasan, Y., Erten, O., & Topal, E. (2018). Accounting for a spatial trend in fine-scale ground-penetrating radar data: A comparative case study. *Journal of the Southern African Institute of Mining and Metallurgy*, 118(2), 173–184. <https://doi.org/10.17159/2411-9717/2018/v118n2a11>
- Dahboosh Al-Shiejiri, S. J. (2013). Investigation of Subsidence Phenomena by GPR Technique and Geotechnical Evaluation in Baghdad City. In *College of Science, Department of Geology: Vol. M SC. UNIVERSITY OF BAGHDAD*.
- Daily, W., & Ramirez, A. (1995). Electrical resistance tomography during in-situ trichloroethylene remediation at the Savannah River Site. *Journal of Applied Geophysics*, 33(4), 239–249. [https://doi.org/10.1016/0926-9851\(95\)90044-6](https://doi.org/10.1016/0926-9851(95)90044-6)

- Dam, R. L. Van. (2001). Causes of ground-penetrating radar reflections in sediment. In *Causes of ground-penetrating radar reflections in sediment*. de Vrije .PhD Thesis. Universiteit Amsterdam.
- Daniels, J. J. (2000). Ground Penetrating Radar Fundamentals. *USEPA Publication, Appendix*, 1–21. [papers2://publication/uuid/B797387B-354B-4A17-98D7-FBEB34EF590B](https://pubs2://publication/uuid/B797387B-354B-4A17-98D7-FBEB34EF590B)
- Daniels, J. J., Roberts, R., & Vendl, M. (1995). Ground penetrating radar for the detection of liquid contaminants. *Journal of Applied Geophysics*, 33(1–3), 195–207. [https://doi.org/10.1016/0926-9851\(95\)90041-1](https://doi.org/10.1016/0926-9851(95)90041-1)
- Darayan, S., Liu, C., Shen, L. C., & Shattuck, D. (1998). Measurement of electrical properties of contaminated soil 1. *Computer, June 1996*, 477–488.
- Davis, J. L., & Annan, a. P. (1989). Ground-Penetrating Radar for High-Resolution Mapping of Soil and Rock Stratigraphy. *Geophysical Prospecting, May 1988*, 531–551. <https://doi.org/10.1111/j.1365-2478.1989.tb02221.x>
- Dawrea, A., Zytner, R. G., & Donald, J. (2021). Enhanced GPR data interpretation to estimate in situ water saturation in a landfill. *Waste Management, 120*, 175–182. <https://doi.org/10.1016/j.wasman.2020.11.033>
- de Benedetto, D., Castrignanò, A., Sollitto, D., & Modugno, F. (2010). Spatial relationship between clay content and geophysical data. *Clay Minerals, 45(2)*, 197–207. <https://doi.org/10.1180/claymin.2010.045.2.197>
- Derek W., T., Steven F., T., Alan O., T., Leharne, S. A., & Gary P., W. (2014). *An illustrated handbook of LNAPL transport and fate in the subsurface* (Michael O. Rivett (Ed.)). Contaminated Land: Applications in Real Environments (CL:AIRE), 32 Bloomsbury Street, London WC1B 3QJL. All. <http://www.claire.co.uk/LNAPL>
- Despotovic, M., Nedic, V., Despotovic, D., & Cvetanovic, S. (2016). Evaluation of empirical models for predicting monthly mean horizontal diffuse solar radiation. *Renewable and Sustainable Energy Reviews, 56*, 246–260. <https://doi.org/10.1016/j.rser.2015.11.058>
- Dhir, R. K., Ghataora, G. S., & Lynn, C. J. (2017). Geotechnical Applications. *Sustainable Construction Materials*, 185–207. <https://doi.org/10.1016/b978-0-08-100987-1.00007-x>

- Dhiware, M., & Corner, C. (2020). Influence of Bulk Density on Dielectric Properties of Soil Samples of Khandesh and Northern Maharashtra. *International Journal of Creative Research Thoughts (IJCRT)*, 6(January 2018).
- DOA, S. S. S. (2018). Common Soil of Peninsular Malaysia: Soil Profile Description and Analytical. In *Soil Resource Management* (1st Editio, Vol. 1). Department of Agriculture Malaysia.
- DOE, B. (2020). *Siasatan kes tumpahan minyak diesel di kawasan perindustrian Tanjung Kidurong, Bintulu, Sarawak*. <https://enviro2.doe.gov.my/>
- Doolittle, J. A., Minzenmayer, F. E., Waltman, S. W., Benham, E. C., Tuttle, J. W., & Peaslee, S. D. (2007). Ground-penetrating radar soil suitability map of the conterminous United States. *Geoderma*, 141(3–4), 416–421. <https://doi.org/10.1016/j.geoderma.2007.05.015>
- Dossi, M., Forte, E., & Pipan, M. (2018). Quantitative Analysis of GPR Signals: Transmitted Wavelet, Amplitude Decay, and Sampling-Related Amplitude Distortions. *Pure and Applied Geophysics*, 175(3), 1103–1122. <https://doi.org/10.1007/s00024-017-1752-2>
- Du, E., Zhao, L., Zou, D., Li, R., Wang, Z., Wu, X., Hu, G., Zhao, Y., Liu, G., & Sun, Z. (2020). Soil moisture calibration equations for active layer GPR detection-a case study specially for the qinghai-tibet plateau permafrost regions. *Remote Sensing*, 12(4). <https://doi.org/10.3390/rs12040605>
- Economou, N., Benedetto, F., Bano, M., Tzanis, A., Nyquist, J., Sandmeier, K. J., & Cassidy, N. (2017). Advanced Ground Penetrating Radar Signal Processing Techniques. *Signal Processing*, 132, 197–200. <https://doi.org/10.1016/j.sigpro.2016.07.032>
- Ehret, B. (2010). Pattern recognition of geophysical data. *Geoderma*, 160(1), 111–125. <https://doi.org/10.1016/j.geoderma.2009.09.008>
- El-Mahallawy, M. S., & Hashim, M. (2013). Material classification of underground utilities from GPR images using DCT-based SVM approach. *IEEE Geoscience and Remote Sensing Letters*, 10(6), 1542–1546. <https://doi.org/10.1109/LGRS.2013.2261796>
- Ercoli, M., Di Matteo, L., Pauselli, C., Mancinelli, P., Frapiccini, S., Talegalli, L., & Cannata, A. (2018). Integrated GPR and laboratory water content measures of sandy soils: From laboratory to field scale. *Construction and Building Materials*, 159, 734–744. <https://doi.org/10.1016/j.conbuildmat.2017.11.082>

- Essam, D., Ahmed, M., Abouelmagd, A., & Soliman, F. (2020). Monitoring temporal variations in groundwater levels in urban areas using ground penetrating radar. *Science of the Total Environment*, 703, 134986. <https://doi.org/10.1016/j.scitotenv.2019.134986>
- Estabragh, A. R., Beytollahpour, I., Moradi, M., & Javadi, A. A. (2014). Consolidation behavior of two fine-grained soils contaminated by glycerol and ethanol. *Engineering Geology*, 178, 102–108. <https://doi.org/10.1016/j.enggeo.2014.05.017>
- Estabragh, A. R., Beytollahpour, I., Moradi, M., & Javadi, A. A. (2016). Mechanical behavior of a clay soil contaminated with glycerol and ethanol. *European Journal of Environmental and Civil Engineering*, 20(5), 503–519. <https://doi.org/10.1080/19648189.2015.1047900>
- Esteve-turrillas, F. A., Pastor, A., & Guardia, M. De. (2012). Passive Sampling of Atmospheric Organic Contaminants. In *Comprehensive Sampling and Sample Preparation: Analytical Techniques for Scientists* (Vol. 1, Issue 1). Elsevier. <https://doi.org/10.1016/B978-0-12-381373-2.10011-0>
- Fan, W., Chang, T., Liu, L., & Cui, H. L. (2017). Dielectric properties of coal in the terahertz frequency region of 100–500 GHz. *Fuel*, 188, 246–253. <https://doi.org/10.1016/j.fuel.2016.10.046>
- Finch, H. J. S., Samuel, A. M., & Lane, G. P. F. (2014). Soils and soil management. *Lockhart & Wiseman's Crop Husbandry Including Grassland*, 37–62. <https://doi.org/10.1533/9781782423928.1.37>
- Firoozy, N., Neusitzer, T., Chirkova, D., Desmond, D. S., Lemes, M. J. L., Landy, J., Mojabi, P., Rysgaard, S., Stern, G., & Barber, D. G. (2018). A controlled experiment on oil release beneath thin sea ice and its electromagnetic detection. *IEEE Transactions on Geoscience and Remote Sensing*, 56(8), 4406–4419. <https://doi.org/10.1109/TGRS.2018.2818717>
- Forte, E., Pipan, M., Casabianca, D., Di Cuia, R., & Riva, A. (2012). Imaging and characterization of a carbonate hydrocarbon reservoir analogue using GPR attributes. *Journal of Applied Geophysics*, 81, 76–87. <https://doi.org/10.1016/j.jappgeo.2011.09.009>
- Francisca, F. M., & Montoro, M. A. (2012). Measuring the dielectric properties of soil-organic mixtures using coaxial impedance dielectric reflectometry. *Journal of Applied Geophysics*, 80, 101–109. <https://doi.org/10.1016/j.jappgeo.2012.01.011>



- Frangi, J. P., Richard, D. C., Chavanne, X., Bexi, I., Sagnard, F., & Guilbert, V. (2009). New in situ techniques for the estimation of the dielectric properties and moisture content of soils. *Comptes Rendus - Geoscience*, 341(10–11), 831–845. <https://doi.org/10.1016/j.crte.2009.08.004>
- Gad, S. C. (2014). Diesel Fuel. In *Encyclopedia of Toxicology: Third Edition* (Third Edit, Vol. 2). Elsevier. <https://doi.org/10.1016/B978-0-12-386454-3.00837-X>
- Gaur, V. K., Niwas, S., & Garg, N. R. (1980). Electrical resistivity anomalies over hydrocarbon bearing structures. *Proceedings of the Indian Academy of Sciences - Earth and Planetary Sciences*, 89(2), 239–248. <https://doi.org/10.1007/BF02913754>
- George, S., Aswathy, E., Berlin, S., Krishnaprabha, N., & Maria, G. (2015). Study on Geotechnical Properties of Diesel Oil Contaminated Soil. *International Journal of Civil and Structural Engineering Research*, 2(2), 113–117. [www.researchpublish.com](http://www.researchpublish.com)
- Giannopoulos, A. (2005). Modelling ground penetrating radar by GprMax. *Construction and Building Materials*, 19(10), 755–762. <https://doi.org/10.1016/j.conbuildmat.2005.06.007>
- Gkortsas, V. M., Venkataramanan, L., Fella, K., Ramsdell, D., Hou, C. Y., & Seleznev, N. (2018). Comparison of different dielectric models to calculate water saturation and estimate textural parameters in partially saturated cores. *Geophysics*, 83(5), E303–E318. <https://doi.org/10.1190/geo2018-0100.1>
- Glaser, D. R., Werkema, D. D., Versteeg, R. J., Henderson, R. D., & Rucker, D. F. (2012). Temporal GPR imaging of an ethanol release within a laboratory-scaled sand tank. *Journal of Applied Geophysics*, 86, 133–145. <https://doi.org/10.1016/j.jappgeo.2012.07.016>
- Gosar, A. (2012). Analysis of the capabilities of low frequency ground penetrating radar for cavities detection in rough terrain conditions: The case of Divača cave, Slovenia. *Acta Carsologica*, 41(1), 77–88. <https://doi.org/10.3986/ac.v41i1.49>
- Guan, S., Liu, W., Liu, W., & Nai, C. (2018). Dielectric Properties Based Detection of Heavy Metal Contaminated Soil in the Frequency Range from 10 MHz to 1 GHz. *Soil and Sediment Contamination*, 27(5), 343–356. <https://doi.org/10.1080/15320383.2018.1474444>

- Guillemoteau, J., Bano, M., & Dujardin, J. R. (2012). Influence of grain size, shape and compaction on georadar waves: Examples of aeolian dunes. *Geophysical Journal International*, *190*(3), 1455–1463. <https://doi.org/10.1111/j.1365-246X.2012.05577.x>
- Guireli Netto, L., Barbosa, A. M., Galli, V. L., Pereira, J. P. S., Gandolfo, O. C. B., & Birelli, C. A. (2020). Application of invasive and non-invasive methods of geo-environmental investigation for determination of the contamination behavior by organic compounds. *Journal of Applied Geophysics*, *178*. <https://doi.org/10.1016/j.jappgeo.2020.104049>
- Guo, B., Song, S., Ghalambor, A., & Lin, T. R. (2014). General Design Information. *Offshore Pipelines*, 13–20. <https://doi.org/10.1016/b978-0-12-397949-0.00002-9>
- Guo, Q., Li, W., Yu, H., & Alvarez, O. (2010). Effects of Topographic Variability and Lidar Sampling Density on Several DEM Interpolation Methods. *Photogrammetric Engineering & Remote Sensing*, *76*(6), 1–12.
- Guo, X., Wang, S., & Wang, X. (2012). Detecting three types of contaminated soil with ground penetrating radar. *2012 14th International Conference on Ground Penetrating Radar, GPR 2012*, 976–980. <https://doi.org/10.1109/icgpr.2012.6255005>
- Hadi Mohammed. (n.d.). Thickness Evaluation of Asphalt and Base Layers of Some Major and Minor Roads in Kumasi Using Ground Penetrating Radar. *International Journal of Scientific & Engineering Research*, *4*, 1–127.
- Hammad, E. A., & Dawelbeit, M. I. (2001). Effect of tillage and field condition on soil physical properties, cane and sugar yields in Vertisols of Kenana Sugar Estate, Sudan. *Soil and Tillage Research*, *62*(3–4), 101–109. [https://doi.org/10.1016/S0167-1987\(01\)00221-5](https://doi.org/10.1016/S0167-1987(01)00221-5)
- Hamzah, U., Ismail, M. A., & Samsudin, A. R. (2009). Geoelectrical resistivity and ground penetrating radar techniques in the study of hydrocarbon-contaminated soil. *Sains Malaysiana*, *38*(3), 305–311.
- Hanaei, F., Sarmadi, M. S., Rezaee, M., & Rahmani, A. (2021). Experimental investigation of the effects of gas oil and benzene on the geotechnical properties of sandy soils. *Innovative Infrastructure Solutions*, *6*(2). <https://doi.org/10.1007/s41062-020-00433-5>

- Haridy, S. A., Persson, M., & Berndtsson, R. (2004). Estimation of LNAPL saturation in fine sand using time-domain reflectometry. *Hydrological Sciences Journal*, 49(6), 987–1000. <https://doi.org/10.1623/hysj.49.6.987.55729>
- Hawari, A., Khader, M., Hirzallah, W., Zayed, T., & Moselhi, O. (2017). Integrated sensing technologies for detection and location of leaks in water distribution networks. *Water Science and Technology: Water Supply*, 17(6), 1589–1601. <https://doi.org/10.2166/ws.2017.044>
- Hendarmawan. (2010). Ground Penetrating Radar ( Gpr ) Survey on the Lava Flow in the Subang Area , West Java Province , Indonesia. *Bulletin of Scientific Contribution*, 8(2), 85–106.
- Hentz, K. L. (2010). Safety Assessment of Pharmaceuticals. *Comprehensive Toxicology, Second Edition*, 3, 17–28. <https://doi.org/10.1016/B978-0-08-046884-6.00303-1>
- Hernández-Mendoza, C. E., García Ramírez, P., & Chávez Alegría, O. (2021). Geotechnical evaluation of diesel contaminated clayey soil. *Applied Sciences (Switzerland)*, 11(14), 1–20. <https://doi.org/10.3390/app11146451>
- Hernández-Mendoza, C. E., García Ramírez, P., Chávez Alegría, O., Ramírez, G., & Alegría, C. (2021). *Geotechnical Evaluation of Diesel Contaminated Clayey Soil Geotechnical Evaluation of Diesel*. <https://doi.org/10.3390/app11146451>
- Hewelke, E., Szatyłowicz, J., Hewelke, P., Gnatowski, T., & Aghalarov, R. (2018a). The Impact of Diesel Oil Pollution on the Hydrophobicity and CO<sub>2</sub> Efflux of Forest Soils. *Water, Air, and Soil Pollution*, 229(2). <https://doi.org/10.1007/s11270-018-3720-6>
- Hewelke, E., Szatyłowicz, J., Hewelke, P., Gnatowski, T., & Aghalarov, R. (2018b). The Impact of Diesel Oil Pollution on the Hydrophobicity and CO<sub>2</sub> Efflux of Forest Soils. *Water Air Soil Pollut*, 51(229). <https://doi.org/10.1007/s11270-018-3720-6>
- Horta, A., Malone, B., Stockmann, U., Minasny, B., Bishop, T. F. A., McBratney, A. B., Pallasser, R., & Pozza, L. (2015). Potential of integrated field spectroscopy and spatial analysis for enhanced assessment of soil contamination: A prospective review. *Geoderma*, 241–242, 180–209. <https://doi.org/10.1016/j.geoderma.2014.11.024>

- Huisman, J. A., Hubbard, S. S., Redman, J. D., & Annan, A. P. (2003). Measuring Soil Water Content with Ground Penetrating Radar: A Review. *Vadose Zone Journal*, 2(4), 476–491. <https://doi.org/10.2136/vzj2003.4760>
- Hung, Y.-C., Lin, C.-P., Lee, C.-T., & Weng, K. (2019). 3D and Boundary Effects on 2D Electrical Resistivity Tomography. *Applied Sciences*, 1–19.
- Indoria, A. K., Sharma, K. L., & Reddy, K. S. (2020). Hydraulic properties of soil under warming climate. In *Climate Change and Soil Interactions*. LTD. <https://doi.org/10.1016/b978-0-12-818032-7.00018-7>
- Iravani, M. A., DeParis, J., Davarzani, H., Colombano, S., Guérin, R., & Mainault, A. (2020). Complex Electrical Resistivity and Dielectric Permittivity Responses to Dense Non-aqueous Phase Liquids' Imbibition and Drainage in Porous Media: A Laboratory Study. *Journal of Environmental and Engineering Geophysics*, 25(4), 557–567. <https://doi.org/10.32389/JEEG20-050>
- Iskandar, R., Tarigan, A. P. M., & Roesyanto, A. P. M. (2018). A Review on the Characteristics of the Smear Zone: Field Data Back Calculation Compared with Laboratory Testing. *The Open Civil Engineering Journal*, 12(1), 340–354. <https://doi.org/10.2174/1874149501812010340>
- Ismail, R. M., Mattarneh, H. M. Al, Fadhil Nuruddin, M., Shafiq, N., & Dahim, M. A. (2017). Dielectric Dispersion Characteristics of Unsaturated Sand Contaminated by Diesel. *Journal of Material Science & Engineering*, 06(03). <https://doi.org/10.4172/2169-0022.1000345>
- Izdebska-Mucha, D., & Trzciński, J. (2021). Clay soil behaviour due to long-term contamination by liquid petroleum fuels: microstructure and geotechnical properties. *Bulletin of Engineering Geology and the Environment*, 80(4), 3193–3206. <https://doi.org/10.1007/s10064-020-02084-3>
- Jacob, R. W., & Urban, T. M. (2016). Ground-Penetrating Radar Velocity Determination and Precision Estimates Using Common-Midpoint (CMP) Collection with Hand-Picking, Semblance Analysis and Cross-Correlation Analysis: A Case Study and Tutorial for Archaeologists. *Archaeometry*, 58(6), 987–1002. <https://doi.org/10.1111/arc.12214>

- Jafery, K. M., Embong, Z., Khee, Y. S., Dahlan, S. H., Ahmad Tajudin, S. A., Ahmad, S., Sahari, S. K., & Maxwell, O. (2018). Investigation of dielectric constant variations for Malaysians soil species towards its natural background dose. *IOP Conference Series: Materials Science and Engineering*, 298(1). <https://doi.org/10.1088/1757-899X/298/1/012003>
- Jat, M. L., Bijay-Singh, Stirling, C. M., Jat, H. S., Tetarwal, J. P., Jat, R. K., Singh, R., Lopez-Ridauro, S., & Shirsath, P. B. (2018). Soil Processes and Wheat Cropping Under Emerging Climate Change Scenarios in South Asia. In *Advances in Agronomy* (1st ed., Vol. 148). Elsevier Inc. <https://doi.org/10.1016/bs.agron.2017.11.006>
- Jia, Y. G., Wu, Q., Shang, H., Yang, Z. N., & Shan, H. X. (2011). The influence of oil contamination on the geotechnical properties of coastal sediments in the Yellow River Delta, China. *Bulletin of Engineering Geology and the Environment*, 70(3), 517–525. <https://doi.org/10.1007/s10064-011-0349-8>
- Jiang, S., Jin, L., Hou, H., & Zhang, L. (2018). Polymer-based nanocomposites with high dielectric permittivity. In *Polymer-Based Multifunctional Nanocomposites and Their Applications*. Elsevier Inc. <https://doi.org/10.1016/B978-0-12-815067-2.00008-1>
- Jin, S., Fallgren, P., Cooper, J., Morris, J., & Urynowicz, M. (2008). Assessment of diesel contamination in groundwater using electromagnetic induction geophysical techniques. *Journal of Environmental Science and Health - Part A Toxic/Hazardous Substances and Environmental Engineering*, 43(6), 584–588. <https://doi.org/10.1080/10934520801893550>
- Jol, H. M., & Bristow, C. S. (2003). GPR in sediments: Advice on data collection, basic processing and interpretation, a good practice guide. *Geological Society Special Publication*, 211, 9–27. <https://doi.org/10.1144/GSL.SP.2001.211.01.02>
- Jordan, T. E., Baker, G. S., Henn, K., & Messier, J. P. (2004). Using amplitude variation with offset and normalized residual polarization analysis of ground penetrating radar data to differentiate an NAPL release from stratigraphic changes. *Journal of Applied Geophysics*, 56(1), 41–58. <https://doi.org/10.1016/j.jappgeo.2004.03.002>
- Jorge, M., & Mesquita, L. (2015). Estimates of Soil Water Content using Ground-Penetrating Radar in Field Conditions. *Brazilian Journal of Geophysic*, 33(3), 1–13.

- Joukar, A., & Boushehrian, A. H. (2020). Experimental Study of Strip Footings Rested on Kerosene Oil- and Gas Oil-Contaminated Sand Slopes. *Iranian Journal of Science and Technology - Transactions of Civil Engineering*, 44(1), 209–217. <https://doi.org/10.1007/s40996-018-00231-1>
- Ju, Z., Sun, H., & Liu, X. (2020). Thermo-time domain reflectometry to evaluate unsaturated soils contaminated with nonaqueous phase liquids. *Vadose Zone Journal*, 19(1), 1–9. <https://doi.org/10.1002/vzj2.20016>
- Kalantar, B., Pradhan, B., Naghibi, S. A., Motevalli, A., & Mansor, S. (2017). Assessment of the effects of training data selection on the landslide susceptibility mapping: a comparison between support vector machine ( SVM ), logistic regression ( LR ) and artificial neural networks ( ANN ). *Geomatics, Natural Hazards and Risk*, 5705(December). <https://doi.org/10.1080/19475705.2017.1407368>
- Kaliakin, V. N. (2017). Example Problems Related to Soil Identification and Classification. In *Soil Mechanics*. <https://doi.org/10.1016/b978-0-12-804491-9.00002-1>
- Karim, G. A. (1980). A review of combustion processes in the dual fuel engine-The gas diesel engine. *Progress in Energy and Combustion Science*, 6(3), 277–285. [https://doi.org/10.1016/0360-1285\(80\)90019-2](https://doi.org/10.1016/0360-1285(80)90019-2)
- Karim, N. I. A., Kamaruddin, S. A., & Hasan, R. C. (2018). Modeling of petrophysical relationship of Soil Water Content estimation at peat lands. *International Journal of Integrated Engineering*, 10(7), 177–187. <https://doi.org/10.30880/ijie.2018.10.07.017>
- Karlina, R., & Sato, M. (2018). Modified Bayesian algorithm implemented in compressive sensing applied to spatially sampled GPR measurement under high clutter conditions. *Nonlinear Theory and Its Applications, IEICE*, 9(1), 121–136. <https://doi.org/10.1587/nolta.9.121>
- Kermani, M., & Ebadi, T. (2012). The Effect of Oil Contamination on the Geotechnical Properties of Fine-Grained Soils. *Soil and Sediment Contamination*, 21(5), 655–671. <https://doi.org/10.1080/15320383.2012.672486>
- Khamehchiyan, M., Hossein Charkhabi, A., & Tajik, M. (2007). Effects of crude oil contamination on geotechnical properties of clayey and sandy soils. *Engineering Geology*, 89(3–4), 220–229. <https://doi.org/10.1016/j.enggeo.2006.10.009>

- Khoshgoftar, A., Khodaparast, M., & Sedighi, M. (2021). Effect of residues from a burnt oil refinery on the compaction parameters and strength of clayey sand. *Bulletin of Engineering Geology and the Environment*, June. <https://doi.org/10.1007/s10064-021-02320-4>
- Khosravi, E., Ghasemzadeh, H., Sabour, M. R., & Yazdani, H. (2013). Geotechnical properties of gas oil-contaminated kaolinite. *Engineering Geology*, *166*, 11–16. <https://doi.org/10.1016/j.enggeo.2013.08.004>
- Kia, S. F., & Abdul, A. S. (1990). Retention of Diesel Fuel in Aquifer Material. *Journal of Hydraulic Engineerin*, *116*(7), 881–894.
- Kimak, C., Ntarlagiannis, D., Slater, L. D., Atekwana, E. A., Beaver, C. L., Rossbach, S., Porter, A., & Ustra, A. (2019). Geophysical Monitoring of Hydrocarbon Biodegradation in Highly Conductive Environments. *Journal of Geophysical Research: Biogeosciences*, *124*(2), 353–366. <https://doi.org/10.1029/2018JG004561>
- Klazinga, D. R., Steelman, C. M., Endres, A. L., & Parker, B. L. (2019). Geophysical response to simulated methane migration in groundwater based on a controlled injection experiment in a sandy unconfined aquifer. *Journal of Applied Geophysics*, *168*, 59–70. <https://doi.org/10.1016/j.jappgeo.2019.05.019>
- Klenk, P. (2012). *Developing Ground-Penetrating Radar for Quantitative Soil Hydrology*. PhD Thesis. Ruperto-Carola University of Heidelberg.
- Klotzsche, A., Jonard, F., Looms, M. C., van der Kruk, J., & Huisman, J. A. (2018). Measuring soil water content with ground penetrating radar: A decade of progress. *Vadose Zone Journal*, *17*(1), 476–491. <https://doi.org/10.2136/vzj2018.03.0052>
- Konečný, F., Boháček, Z., Müller, P., Kovářová, M., & Sedláčková, I. (2003). Contamination of soils and groundwater by petroleum hydrocarbons and volatile organic compounds - Case study: ELSLAV BRNO. *Bulletin of Geosciences*, *78*(3), 225–239. <https://doi.org/10.3140/bull.geosci.2003.03.225>
- Koyama, C. N., Liu, H., Takahashi, K., Shimada, M., Watanabe, M., Khuut, T., & Sato, M. (2017). In-situ measurement of soil permittivity at various depths for the calibration and validation of low-frequency SAR soil moisture models by using GPR. *Remote Sensing*, *9*(6), 1–14. <https://doi.org/10.3390/rs9060580>

- Kumar Rai, R., Vijay, P. S., & Upadhyay, A. (2017). Soil analysis. *Planning and Evaluation of Irrigation Projects (Methods and Implementation)*, 505–523. <https://doi.org/10.1016/B978-0-12-811748-4.00017-0>
- Lai, W. W. L., Chang, R. K. W., Sham, J. F. C., & Pang, K. (2016). Perturbation mapping of water leak in buried water pipes via laboratory validation experiments with high-frequency ground penetrating radar (GPR). *Tunnelling and Underground Space Technology*, 52, 157–167. <https://doi.org/10.1016/j.tust.2015.10.017>
- Lanza, N. L., & Newsom, H. E. (2013). Extraterrestrial Hillslope Processes. In *Treatise on Geomorphology* (Vol. 7). Elsevier Ltd. <https://doi.org/10.1016/B978-0-12-374739-6.00188-3>
- Latif, S. N. A., Chiong, M. S., Rajoo, S., Takada, A., Chun, Y. Y., Tahara, K., & Ikegami, Y. (2021). The trend and status of energy resources and greenhouse gas emissions in the Malaysia power generation mix. *Energies*, 14(8), 1–26. <https://doi.org/10.3390/en14082200>
- Lenhard, R. J., Dane, J. H., & Oostrom, M. (2004). Immiscible Fluids. *Encyclopedia of Soils in the Environment*, 4, 239–247. <https://doi.org/10.1016/B0-12-348530-4/00571-3>
- Leucci, G. (2008). Ground Penetrating Radar: The Electromagnetic Signal Attenuation and Maximum Penetration Depth. *Scholarly Research Exchange*, 2008, 1–7. <https://doi.org/10.3814/2008/926091>
- Li, Y., Zhou, L., Chen, J., Subbiah, J., Chen, X., Fu, H., & Wang, Y. (2018). Dielectric properties of chili powder in the development of radio frequency and microwave pasteurisation. *International Journal of Food Properties*, 20(3), S3373–S3384. <https://doi.org/10.1080/10942912.2017.1358745>
- Ling, D., Zhao, Y., Wang, Y., & Huang, B. (2016). Study on relationship between dielectric constant and water content of rock-soil mixture by time domain reflectometry. *Journal of Sensors*, 2016. <https://doi.org/10.1155/2016/2827890>
- Liu, H., Deng, Z., Han, F., Xia, Y., Liu, Q. H., & Sato, M. (2017). Time-frequency analysis of air-coupled GPR data for identification of delamination between pavement layers. *Construction and Building Materials*, 154, 1207–1215. <https://doi.org/10.1016/j.conbuildmat.2017.06.132>



- Liu, H., Lin, C., Cui, J., Fan, L., Xie, X., & Spencer, B. F. (2020). Detection and localization of rebar in concrete by deep learning using ground penetrating radar. *Automation in Construction*, *118*, 103279. <https://doi.org/10.1016/j.autcon.2020.103279>
- Liu, S., Lu, Q., Li, H., & Wang, Y. (2020). Estimation of moisture content in railway subgrade by ground penetrating radar. *Remote Sensing*, *12*(18), 1–15. <https://doi.org/10.3390/RS12182912>
- Liu, X., Dong, X., Xue, Q., Leskovar, D. I., Jifon, J., Butnor, J. R., & Marek, T. (2018). Ground penetrating radar (GPR) detects fine roots of agricultural crops in the field. *Plant and Soil*, *423*(1–2), 517–531. <https://doi.org/10.1007/s11104-017-3531-3>
- Liu, X., Hao, P., Wang, A., Zhang, L., Gu, B., & Lu, X. (2021). Non-destructive detection of highway hidden layer defects using a groundpenetrating radar and adaptive particle swarm support vector machine. *PeerJ Computer Science*, *7*, 1–18. <https://doi.org/10.7717/PEERJ-CS.417>
- Loewer, M., Günther, T., Igel, J., Kruschwitz, S., Martin, T., & Wagner, N. (2017). Ultra-broad-band electrical spectroscopy of soils and sediments—a combined permittivity and conductivity model. *Geophysical Journal International*, *210*(3), 1360–1373. <https://doi.org/10.1093/gji/ggx242>
- Lorah, M. M., Majcher, E. H., & Morel, C. J. (2019). Effective Solubility Assessment for Organic Analytes in Liquid Samples , BKK Class I Landfill , West Covina , California , 2014 – 16. In *Open-File Report 2019–1080: U.S. Department of the Interior and U.S. Geological Survey*. <https://pubs.usgs.gov/of/2019/1080/ofr20191080.pdf>
- Lu, Y., Song, W., Lu, J., Wang, X., & Tan, Y. (2017). An examination of soil moisture estimation using ground penetrating radar in desert steppe. *Water (Switzerland)*, *9*(7), 1–11. <https://doi.org/10.3390/w9070521>
- Mala Geoscience AB. (2009). *GroundVision Software Operating Manual v. 1.4*. MALA Geoscience AB. [www.malags.com](http://www.malags.com)
- Mallet, F., Carrière, S. D., Chalikakis, K., & Marc, V. (2018). Assessing soil water content spatio-temporal variability at the hillslope scale in a headwater catchment using a multi variable interpolation model based on EMI surveys (Draix, South Alps, France). *Environmental Earth Sciences*, *77*(13), 0. <https://doi.org/10.1007/s12665-018-7687-9>

- Manataki, M., Sarris, A., Donati, J. C., Garcia, C. C., & Kalayci, T. (2019). GPR: Theory and practice in archaeological prospection. *New Global Perspectives on Archaeological Prospection*, December, 13–24. <https://doi.org/10.13140/RG.2.1.3256.9363>
- Mansi, A. H., Castillo, M. P., & Bernasconi, G. (2017). Controlled laboratory test for the investigation of LNAPL contamination using a 2.0 GHz ground penetrating radar. *Bollettino Di Geofisica Teorica Ed Applicata*, 58(3), 169–180. <https://doi.org/10.4430/bgta0197>
- Mao, J., Liu, J., Wang, H., Yang, X., Zhang, Z., Yang, B., & Zhao, J. (2017). Novel terpolymers as viscosity reducing agent for Tahe super heavy oil. *RSC Advances*, 7(31), 19257–19261. <https://doi.org/10.1039/c7ra00508c>
- Martinez, A., & Byrnes, A. P. (2001). Modeling dielectric-constant values of geologic materials: An aid to ground-penetrating radar data collection and interpretation. *Current Research in Earth Sciences*, 247(1), 1–16.
- Mazurek, E. (2012). Practical Application of High Resolution Ground Penetrating Radar Method Inside Buildings. *Geol Geophys Environ*, 38(4), 439–448.
- Mcnaughton, C. H. (2011). *Monitoring a Shallow Gasoline Release using GPR at CFB Borden*. Master Thesis. University of Waterloo.
- McWatters, R. S., Rowe, R. K., Wilkins, D., Spedding, T., Hince, G., Richardson, J., & Snape, I. (2019). Modelling of vapour intrusion into a building impacted by a fuel spill in Antarctica. *Journal of Environmental Management*, 231(July 2018), 467–482. <https://doi.org/10.1016/j.jenvman.2018.07.092>
- Mechbal, Z., & Khamlichi, A. (2017). Determination of concrete rebars characteristics by enhanced post-processing of GPR scan raw data. *NDT and E International*, 89, 30–39. <https://doi.org/10.1016/j.ndteint.2017.03.005>
- Mercer, R. M. C. & J. W. (1993). DNAPL Site Evaluation. *USEPA Publication, EPA/600/R-*, 1–369. [papers2://publication/uuid/2DA59CBF-D34D-4A7E-AAE9-155A011FE070](https://pubs2://publication/uuid/2DA59CBF-D34D-4A7E-AAE9-155A011FE070)
- Meyer, R., Thompson, J. S., Kelly, B. M., Khatiwada, M., Harris, J. M., Quan, Y., Wynn, D., Ajo-franklin, J., Wu, C., Urban, J., Akintunde, O. M., Lerat, O., Adjemian, F., Baroni, A., Etienne, G., Renard, G., Bathellier, E., Forgues, E., Aubin, F., ... Ivanova, A. (2013). Subsurface Monitoring of Geological CO<sub>2</sub> Storage. *Geophysics*, 66(1), 116–127. <https://doi.org/10.1190/1.1444903>

- Millington, T. M., & Cassidy, N. J. (2010). Optimising GPR modelling: A practical, multi-threaded approach to 3D FDTD numerical modelling. *Computers and Geosciences*, 36(9), 1135–1144. <https://doi.org/10.1016/j.cageo.2009.12.006>
- Mironov, V. L., Kosolapova, L. G., Fomin, S. V., & Savin, I. V. (2019). Experimental analysis and empirical model of the complex permittivity of five organic soils at 1.4 GHz in the Temperature Range from -30 °c to 25 °c. *IEEE Transactions on Geoscience and Remote Sensing*, 57(6), 3778–3787. <https://doi.org/10.1109/TGRS.2018.2887117>
- Mishra, P. N., Bore, T., Jiang, Y., Scheuermann, A., & Li, L. (2018). Dielectric spectroscopy measurements on kaolin suspensions for sediment concentration monitoring. *Measurement: Journal of the International Measurement Confederation*, 121(January), 160–169. <https://doi.org/10.1016/j.measurement.2018.02.034>
- Mitchum, R. M., Vail, P. R., & Sangree, J. B. (1977). Seismic stratigraphy and global changes of sea Level, part 6: Stratigraphic interpretation of seismic reflection patterns in depositional sequences. *Seismic Stratigraphy - Applications to Hydrocarbon Exploration*, 117–134.
- Mobilian, C., & Craft, C. B. (2022). Wetland Soils: Physical and Chemical Properties and Biogeochemical Processes. *Reference Module in Earth Systems and Environmental Sciences*, 157–168. <https://doi.org/10.1016/B978-0-12-819166-8.00049-9>
- Mohamed, I. S. (2022, May 12). Bengkel lori disyaki punca pencemaran minyak diesel. *Kosmo Malaysia*, 2022. Retrieved June 12, 2022 from <https://www.kosmo.com.my/2022/05/12/bengkel-lori-disyaki-punca-pencemaran-minyak-diesel/>
- Moorman, B. J. (2005). Ground-Penetrating Radar Applications in Paleolimnology. *Tracking Environmental Change Using Lake Sediments*, 23–47. [https://doi.org/10.1007/0-306-47669-x\\_3](https://doi.org/10.1007/0-306-47669-x_3)
- Mount, G. J., Comas, X., Wright, W. J., & McClellan, M. D. (2015). Delineation of macroporous zones in the unsaturated portion of the Miami Limestone using ground penetrating radar, Miami Dade County, Florida. *Journal of Hydrology Journal*, 527, 872–883. <https://doi.org/10.1016/j.jhydrol.2015.05.053>

- Mueller, S., Dennison, G., & Liu, S. (2021). An assessment on ethanol-blended gasoline/diesel fuels on cancer risk and mortality. *International Journal of Environmental Research and Public Health*, 18(13). <https://doi.org/10.3390/ijerph18136930>
- Mulla, D. J. (2012). Modeling and Mapping Soil Spatial and Temporal Variability. In *Hydropedology*. Elsevier B.V. <https://doi.org/10.1016/B978-0-12-386941-8.00020-4>
- Muniappan, N., & Balasubramani, D. (2011). 3D Subsurface Mapping and Classification using GPR and Support Vector Machines for Cylindrical Object Identificatio. *International Conference on Civil, Structural, and Environmental Engineering, February*.
- Musa, A. B. (2013). Comparative study on classification performance between support vector machine and logistic regression. *Int. J. Mach. Learn. & Cyber.*, 4, 13–24. <https://doi.org/10.1007/s13042-012-0068-x>
- Mustafa, B., Doruk, E., Basak, A., & Engin, A. (2020). The effect of environmental diesel exhaust pollution on SARS-CoV-2 infection: The mechanism of pulmonary ground glass opacity. *Environmental Toxicology and Pharmacology*, January.
- Nadler, A., Dasberg, S., & Lapid, I. (1991). Time Domain Reflectometry Measurements of Water Content and Electrical Conductivity of Layered Soil Columns”. *Soil Science Society of America Journal*, 57(5), 1396–1396. <https://doi.org/10.2136/sssaj1993.03615995005700050042x>
- Nagano, S., Yamamoto, S., Nagakubo, M., Atsumi, K., & Watanabe, M. M. (2012). Physical Properties of Hydrocarbon Oils Produced by Botryococcus Braunii: Density, Kinematic Viscosity, Surface Tension, and Distillation Properties. *Procedia Environmental Sciences*, 15, 73–79. <https://doi.org/10.1016/j.proenv.2012.05.012>
- Nasehi, S. A., Uromeihy, A., Nikudel, M. R., & Morsali, A. (2016). Influence of Gas Oil Contamination on Geotechnical Properties of Fine and Coarse-Grained Soils. *Geotechnical and Geological Engineering*, 34(1), 333–345. <https://doi.org/10.1007/s10706-015-9948-7>

- Nasr, A. M. A. (2010). Experimental and theoretical studies for the behavior of strip footing on oil-contaminated sand. *Journal of Geotechnical and Geoenvironmental Engineering*, 135(12), 1814–1822. [https://doi.org/10.1061/\(ASCE\)GT.1943-5606.0000165](https://doi.org/10.1061/(ASCE)GT.1943-5606.0000165)
- Naveen, B. P., & Malik, R. K. (2019). Assessment of contamination potential of leachate from municipal solid waste landfill sites for metropolitan cities in India. *Pollution*, 5(2), 313–322. <https://doi.org/10.22059/poll.2018.266991.527>
- Nelson, S. O. (2004). Dielectric properties and density relationships for granular materials. *ASAE Annual International Meeting 2004*, 0300(04), 6767–6775. <https://doi.org/10.13031/2013.17891>
- Nimmo, J. R. (2013). Porosity and Pore Size Distribution. In *Reference Module in Earth Systems and Environmental Sciences*. Published by Elsevier Inc. <https://doi.org/10.1016/b978-0-12-409548-9.05265-9>
- Ninje, D. J. (2017). *Treatment, Processing and Interpretation of GPR Data Acquired From the Archaeological Site of Castro De UL, Northern Portugal* (Issue October). Master Thesis. University of Porto.
- Nishimoto, M., Kimura, Y., & Tanaka, T. (2006). A Three-Dimensional Feature Vector for Identification of Buried Landmines Using GPR Data. *International Symposium on Antennas and Propagation* —, 1–5.
- Noon, D. A., Stickley, G. F., & Longstaff, D. (1998). A frequency-independent characterisation of GPR penetration and resolution performance. *Journal of Applied Geophysics*, 40(1–3), 127–137. [https://doi.org/10.1016/S0926-9851\(98\)00008-1](https://doi.org/10.1016/S0926-9851(98)00008-1)
- Nouri, M., Homaei, M., & Bybordi, M. (2014). Quantitative Assessment of LNAPL Retention in Soil Porous Media. *Soil and Sediment Contamination*, 23(8), 801–819. <https://doi.org/10.1080/15320383.2014.887650>
- Olchawa, A., & Kumor, M. (2008). Time domain reflectometry (tdr) - measuring dielectric constant of polluted soil to estimate diesel oil content. *Archives of Hydroengineering and Environmental Mechanics*, 55(1–2), 55–62.
- Olgun, M., & Yildiz, M. (2010). Effect of organic fluids on the geotechnical behavior of a highly plastic clayey soil. *Applied Clay Science*, 48(4), 615–621. <https://doi.org/10.1016/j.clay.2010.03.015>

- Orru, E., Durbiano, F., & Ortolano, M. (2014). Traceability of electrolytic conductivity measurements for ultra pure water. *Accred Qual Assur*, *19*, 11–16. <https://doi.org/10.6092/polito/porto/2553145>
- Osinowo, O. O., Falufosi, M. O., & Omiyale, E. O. (2018). Integrated electromagnetic (EM) and Electrical Resistivity Tomography (ERT) geophysical studies of environmental impact of Awotan dumpsite in Ibadan, southwestern Nigeria. *Journal of African Earth Sciences*, *140*, 42–51. <https://doi.org/10.1016/j.jafrearsci.2017.12.026>
- Owenier, F., Hornung, J., & Hinderer, M. (2018). Substrate-sensitive relationships of dielectric permittivity and water content: implications for moisture sounding. *Near Surface Geophysics*, *16*(2), 128–152. <https://doi.org/10.3997/1873-0604.2017050>
- Pakparvar, M., Cornelis, W., Gabriels, D., Mansouri, Z., & Kowsar, S. A. (2016). Enhancing modelled water content by dielectric permittivity in stony soils. *Soil Research*, *54*(3), 360–370. <https://doi.org/10.1071/SR15154>
- Palneedi, H., Peddigari, M., Upadhyay, A., Silva, J. P. B., Hwang, G.-T., & Ryu, J. (2021). Lead-based and lead-free ferroelectric ceramic capacitors for electrical energy storage. In *Ferroelectric Materials for Energy Harvesting and Storage*. <https://doi.org/10.1016/b978-0-08-102802-5.00009-1>
- Panchami, M. V., Bindu, J., & Kannan, K. (2021). Effect of Oil Contamination on Geotechnical Properties of Lateritic Soils. In *Lecture Notes in Civil Engineering* (Vol. 88). Springer Singapore. [https://doi.org/10.1007/978-981-15-6237-2\\_22](https://doi.org/10.1007/978-981-15-6237-2_22)
- Park, C. H., Behrendt, A., LeDrew, E., & Wulfmeyer, V. (2017). New approach for calculating the effective dielectric constant of the moist soil for microwaves. *Remote Sensing*, *9*(7), 1–30. <https://doi.org/10.3390/rs9070732>
- Pasolli, E., Melgani, F., & Donelli, M. (2009). Automatic analysis of GPR images: A pattern-recognition approach. *IEEE Transactions on Geoscience and Remote Sensing*, *47*(7), 2206–2217. <https://doi.org/10.1109/TGRS.2009.2012701>
- Pasolli, E., Melgani, F., Donelli, M., Attoui, R., & De Vos, M. (2008). Automatic detection and classification of buried objects in GPR images using genetic algorithms and support vector machines. *International Geoscience and Remote Sensing Symposium (IGARSS)*, *2*(1), 525–528. <https://doi.org/10.1109/IGARSS.2008.4779044>

- Patriarca, C., Tosti, F., Velds, C., Benedetto, A., Lambot, S., & Slob, E. (2013). Frequency dependent electric properties of homogeneous multi-phase lossy media in the ground-penetrating radar frequency range. *Journal of Applied Geophysics*, 97, 81–88. <https://doi.org/10.1016/j.jappgeo.2013.05.003>
- Paula Castilo, M. (2015). *Using ground penetrating radar in the investigation of LNAPL contamination within a controlled environment* (Issue APRIL 2013). Master Thesis. Polytechnic of Milano. <https://doi.org/10.13140/RG.2.1.3228.6565>
- Paula, M., & Politecnico, C. (2015). *Using ground penetrating radar in the investigation of LNAPL contamination within a controlled environment. APRIL 2013*. <https://doi.org/10.13140/RG.2.1.3228.6565>
- Pellinen, T., Huuskonen-Snicker, E., Eskelinen, P., & Olmos Martinez, P. (2015). Representative volume element of asphalt pavement for electromagnetic measurements. *Journal of Traffic and Transportation Engineering (English Edition)*, 2(1), 30–39. <https://doi.org/10.1016/j.jtte.2015.01.003>
- Piuzzi, E., Cannazza, G., Cataldo, A., De Benedetto, E., De Giorgi, L., Frezza, F., Leucci, G., Pisa, S., Pittella, E., Prontera, S., & Timpani, F. (2018). A comparative assessment of microwave-based methods for moisture content characterization in stone materials. *Measurement: Journal of the International Measurement Confederation*, 114, 493–500. <https://doi.org/10.1016/j.measurement.2016.04.046>
- Polit, E. (2017). *Development of Signal Ground-Penetrating Radar to Evaluate the Quality of Stone*. PhD Thesis. University of Giennensis.
- Porsani, J. L., Filho, W. M., Elis, V. R., Shimeles, F., Dourado, J. C., & Moura, H. P. (2004). The use of GPR and VES in delineating a contamination plume in a landfill site: A case study in SE Brazil. *Journal of Applied Geophysics*, 55(3–4), 199–209. <https://doi.org/10.1016/j.jappgeo.2003.11.001>
- Porubiaková, A., & Komačka, J. (2015). A comparison of dielectric constants of various asphalts calculated from time intervals and amplitudes. *Procedia Engineering*, 111(TFoCE), 660–665. <https://doi.org/10.1016/j.proeng.2015.07.129>
- Qiao, X., Yang, F., & Zheng, J. (2019). Ground penetrating radar weak signals denoising via semi-soft threshold empirical wavelet transform. *Ingenierie Des Systemes d'Information*, 24(2), 207–213. <https://doi.org/10.18280/isi.240213>

- Radziemska, M., & Fronczyk, J. (2015). Level and contamination assessment of soil along an expressway in an ecologically valuable area in Central Poland. *International Journal of Environmental Research and Public Health*, *12*(10), 13372–13387. <https://doi.org/10.3390/ijerph121013372>
- Rajapakse, R. (2016). Soil laboratory testing. *Geotechnical Engineering Calculations and Rules of Thumb*, *200*(200), 47–60. <https://doi.org/10.1016/b978-0-12-804698-2.00004-0>
- Ramesh, T., Bolan, N. S., Kirkham, M. B., Wijesekara, H., Kanchikerimath, M., Srinivasa Rao, C., Sandeep, S., Rinklebe, J., Ok, Y. S., Choudhury, B. U., Wang, H., Tang, C., Wang, X., Song, Z., & Freeman, O. W. (2019). Soil organic carbon dynamics: Impact of land use changes and management practices: A review. *Advances in Agronomy*, *156*, 1–107. <https://doi.org/10.1016/bs.agron.2019.02.001>
- Rao, C. S., & Chandrashekhara, V. (2014). Detecting oil contamination by Ground Penetrating Radar around an oil storage facility in Dhanbad, Jharkhand, India. *J. Ind. Geophys. Union*, *18*(4), 448–454. <https://doi.org/10.4016/28481.01>
- Rashed, M. A., & Al-Garni, M. A. (2013). On the application of GPR for locating underground utilities in urban areas. *Arabian Journal of Geosciences*, *6*(9), 3505–3511. <https://doi.org/10.1007/s12517-012-0588-4>
- Rasol, M., Pérez-Gracia, V., & Assunção, S. S. (2018). Analysis and Calibration of Ground Penetrating Radar Shielded Antennas. *2018 17th International Conference on Ground Penetrating Radar, GPR 2018, June*. <https://doi.org/10.1109/ICGPR.2018.8441541>
- Redman, J. D. (2009). *Chapter 8 - Contaminant Mapping* (H. M. B. T.-G. P. R. T. and A. Jol (Ed.); pp. 247–269). Elsevier. <https://doi.org/10.1016/B978-0-444-53348-7.00008-9>
- Regmi, N. R., Giardino, J. R., McDonald, E. V., & Vitek, J. D. (2015). A Review of Mass Movement Processes and Risk in the Critical Zone of Earth. In *Developments in Earth Surface Processes* (Vol. 19). Elsevier B.V. <https://doi.org/10.1016/B978-0-444-63369-9.00011-2>
- Rehman, F., Abouelnaga, H. S. O., & Rehman, F. (2016). Estimation of dielectric permittivity, water content, and porosity for environmental engineering and hydrogeological studies using ground penetrating radar, a short review. *Arabian Journal of Geosciences*, *9*(4), 1–7. <https://doi.org/10.1007/s12517-016-2328-7>



- Rhodes, C. J. (2013). Feeding and healing the world: Through regenerative agriculture and permaculture. *Science Progress*, 95(4), 345–446. <https://doi.org/10.3184/003685012X13504990668392>
- Robinson, M., Bristow, C., Mckinley, J., & Ruffell, A. (2013). Section 1.5.5 Ground Penetrating Radar. In *British Society of Geomorphology* (Vol. 5, pp. 1–26).
- Robinson, M., Bristow, C., McKinley, J., & Ruffell, A. (2013). Section 1.5.5 Ground Penetrating Radar. *Geomorphological Techniques (Online Edition)*, 5, 1–26.
- Roth, C. H., Malicki, M. A., & Plagge, R. (1992). Empirical evaluation of the relationship between soil dielectric constant and volumetric water content as the basis for calibrating soil moisture measurements by TDR. *Journal of Soil Science*, 43(1), 1–13. <https://doi.org/10.1111/j.1365-2389.1992.tb00115.x>
- Roth, K., Schulin, R., Flühler, H., & Attinger, W. (1990). Calibration of time domain reflectometry for water content measurement using a composite dielectric approach. *Water Resources Research*, 26(10), 2267–2273. <https://doi.org/10.1029/WR026i010p02267>
- Rubin, A. J., & Ho, C. L. (2018). A Review of Empirical Methods to Estimate Relative Permittivity. *2018 17th International Conference on Ground Penetrating Radar, GPR 2018*. <https://doi.org/10.1109/ICGPR.2018.8441646>
- S.Paramananthan. (2020). Malaysia Soil Taxonomy. In *Agricultural Crop Trust* (3rd Editio, Vol. 1, Issue 1). Param Agricultural Soil Surveys (M) Sdn.Bhd.
- Saint-Laurent, D., & Arsenault-Boucher, L. (2020). Properties of alluvial and non-alluvial soils in fragmented mixed deciduous forest patches in southern Québec, Canada. *Catena*, 184(October 2019), 104254. <https://doi.org/10.1016/j.catena.2019.104254>
- Salat, C., & Junge, A. (2010). Dielectric permittivity of fine-grained fractions of soil samples from eastern Spain at 200 MHz. *Geophysics*, 75(1). <https://doi.org/10.1190/1.3294859>
- Salih, S. A. (2003). Applications of Ground Penetrating Radar (GPR) in Detection of Groundwater Table Near Pumping Well. *Tikrit Journal of Pure Science*, 12(1), 1–16.
- Sandmeier, K. (2017). *Introduction to the processing of GPR-data within REFLEXW*. <https://www.sandmeier-geo.de/>

- Šarlah, N., Podobnikar, T., Mongus, D., Ambrožič, T., & Mušič, B. (2019). Kinematic GPR-TPS model for infrastructure asset identification with high 3D georeference accuracy developed in a real urban test field. *Remote Sensing*, *11*(12). <https://doi.org/10.3390/rs11121457>
- Sauck, W. A. (2000). A model for the resistivity structure of LNAPL plumes and their environs in sandy sediments. *Journal of Applied Geophysics*, *44*(2–3), 151–165. [https://doi.org/10.1016/S0926-9851\(99\)00021-X](https://doi.org/10.1016/S0926-9851(99)00021-X)
- Schaschke, C., Fletcher, I., & Glen, N. (2013). Density and viscosity measurement of diesel fuels at combined high pressure and elevated temperature. *Processes*, *1*(2), 30–48. <https://doi.org/10.3390/pr1020030>
- Seyfried, M. S., & Grant, L. E. (2007). Temperature Effects on Soil Dielectric Properties Measured at 50 MHz. *Vadose Zone Journal*, *6*(4), 759–765. <https://doi.org/10.2136/vzj2006.0188>
- Shaaban, F., Habeebullah, T. M., Morsy, E. A., & Gabr, S. (2016). Ground penetrating radar and 2D electric resistivity studies for tracing hydrocarbon leakage site, close to Abha City: a case study. *Arabian Journal of Geosciences*, *9*(20). <https://doi.org/10.1007/s12517-016-2706-1>
- Sham, J. F. C., & Lai, W. W. L. (2015). A new algorithm for more accurate estimation of wave propagation velocity by common-offset survey method. *International Symposium on Non-Destructive Testing in Civil Engineering (NDT-CE)*.
- Shamir, O., Goldshleger, N., Basson, U., & Reshef, M. (2018). Laboratory measurements of subsurface spatial moisture content by ground-penetrating radar (GPR) diffraction and reflection imaging of agricultural soils. *Remote Sensing*, *10*(10). <https://doi.org/10.3390/rs10101667>
- Shao, S., Gao, C., Guo, X., Wang, Y., Zhang, Z., Yu, L., & Tang, H. (2019). Mapping the contaminant plume of an abandoned hydrocarbon disposal site with geophysical and geochemical methods, Jiangsu, China. *Environmental Science and Pollution Research*, *26*(24), 24645–24657. <https://doi.org/10.1007/s11356-019-05780-0>
- Shao, S., Guo, X., & Ding, H. (2019). Temporal ground penetrating radar (GPR) imaging of an oil release within a porous medium: A description of anomalous GPR characteristics during the degradation process and a contaminated area determination method. In *Environmental Science and Engineering*. Springer Singapore. [https://doi.org/10.1007/978-981-13-2221-1\\_97](https://doi.org/10.1007/978-981-13-2221-1_97)

- Shao, W., Bouzerdoum, A., & Phung, S. L. (2011). Sparse signal decomposition for ground penetrating radar. *2011 IEEE RadarCon (RADAR)*, 453–457. <https://doi.org/10.1109/RADAR.2011.5960579>
- Shao, W., Bouzerdoum, A., Phung, S. L., Su, L., Indraratna, B., & Rujikiatkamjom, C. (2010). Automatic classification of GPR signals. *Proceedings of the 13th International Conference on Ground Penetrating Radar, GPR 2010*. <https://doi.org/10.1109/ICGPR.2010.5550187>
- Sharma, R. K. (2014). *Effect Of Diesel Pollution On Sub-Grade And Permeability Characteristics Of Fly Ash-Sand Composite*. 451–461.
- Shrestha, S. M., & Arai, I. (2003). Signal processing of ground penetrating radar using spectral estimation techniques to estimate the position of buried targets. *Eurasip Journal on Applied Signal Processing*, 2003(12), 1198–1209. <https://doi.org/10.1155/S1110865703307036>
- Smitha, N., & Singh, V. (2020). Target detection using supervised machine learning algorithms for GPR data. *Sensing and Imaging*, 21(1), 1–15. <https://doi.org/10.1007/s11220-020-0273-8>
- Sonkamble, S., & Chandra, S. (2021). GPR for earth and environmental applications: Case studies from India. *Journal of Applied Geophysics*, 193(October 2020), 104422. <https://doi.org/10.1016/j.jappgeo.2021.104422>
- Srigutomo, W., Trimadona, & Agustine, E. (2016). Investigation of Underground Hydrocarbon Leakage using Ground Penetrating Radar. *Journal of Physics: Conference Series*, 739(1). <https://doi.org/10.1088/1742-6596/739/1/012137>
- Steelman, C. M., & Endres, A. L. (2011). Comparison of petrophysical relationships for soil moisture estimation using GPR ground waves. *Vadose Zone Journal*, 10(1), 270–285. <https://doi.org/10.2136/vzj2010.0040>
- Sutton, N. B., Maphosa, F., Morillo, J. A., Al-Soud, W. A., Langenhoff, A. A. M., Grotenhuis, T., Rijnaarts, H. H. M., & Smidt, H. (2013). Impact of long-term diesel contamination on soil microbial community structure. *Applied and Environmental Microbiology*, 79(2), 619–630. <https://doi.org/10.1128/AEM.02747-12>
- Syafalni, S., Dhaarisheni, M., Abustan, I., & Mohd Remy Rozainy, M. A. Z. (2015). Landfill leachate treatment by using peat soil and laterite soil as natural adsorbents. *International Journal of Applied Engineering Research*, 10(3), 5707–5728.

- Szyplowska, A., Szerement, J., Lewandowski, A., Kafarski, M., Wilczek, A., & Skierucha, W. (2018). Impact of Soil Salinity on the Relation between Soil Moisture and Dielectric Permittivity. *2018 12th International Conference on Electromagnetic Wave Interaction with Water and Moist Substances, ISEMA 2018*, 1–3. <https://doi.org/10.1109/ISEMA.2018.8442298>
- Taflove, A., & Hagness, S. C. (2005). *The Finite-Difference Time-Domain Method Third Edition* (3rd Editio). Artech House.
- Tarvainen, V., & Forsén, H. (2000). Accuracy and functionality of hand held wood moisture content meters. *Vtt Publications*, 102. <http://www.inf.vtt.fi/pdf/>
- Tempke, R., Wildfire, C., Shekhawat, D., & Musho, T. (2018). *Experimental Measurement of Dielectric Properties of Powdery Materials using a Coaxial Transmission Line*. 1–9.
- Terry, N., Day-Lewis, F. D., Lane, J. W., Trost, J. J., & Bekins, B. A. (2019). Geophysical mapping of plume discharge to surface water at a crude oil spill site: Inversion versus machine learning. *Geophysics*, 84(5), EN67–EN80. <https://doi.org/10.1190/geo2018-0690.1>
- Thankam, N. S., Rekha, V., & Shankar, U. (2017). Use of lateritic soil amended with bentonite as landfill liner. *Rasayan Journal of Chemistry*, 10(4), 1431–1438. <https://doi.org/10.7324/RJC.2017.1041818>
- Tillard, S., & Dubois, J. C. (1995). Analysis of GPR data: wave propagation velocity determination. *Journal of Applied Geophysics*, 33(1–3), 77–91. [https://doi.org/10.1016/0926-9851\(95\)90031-4](https://doi.org/10.1016/0926-9851(95)90031-4)
- Todkar, S. S., Baltazart, V., Ihamouten, A., Dérobert, X., & Guilbert, D. (2021). One-class SVM based outlier detection strategy to detect thin interlayer debondings within pavement structures using Ground Penetrating Radar data. *Journal of Applied Geophysics*, 192. <https://doi.org/10.1016/j.jappgeo.2021.104392>
- Topp, G. C., Davis, J. L., & Annan, A. P. (1980). Electromagnetic determination of soil water content: Measurements in coaxial transmission lines. *Water Resources Research*, 16(3), 574–582. <https://doi.org/10.1029/WR016i003p00574>
- Tosti, F., Patriarca, C., Slob, E., Benedetto, A., & Lambot, S. (2013). Clay content evaluation in soils through GPR signal processing. *Journal of Applied Geophysics*, 97, 69–80. <https://doi.org/10.1016/j.jappgeo.2013.04.006>

- Travassos, X. L., Avila, S. L., & Ida, N. (2018). Artificial Neural Networks and Machine Learning techniques applied to Ground Penetrating Radar: A review. *Applied Computing and Informatics*, 1–7. <https://doi.org/10.1016/j.aci.2018.10.001>
- Travassos, X. L., Avila, S. L., & Ida, N. (2021). Artificial Neural Networks and Machine Learning techniques applied to Ground Penetrating Radar: A review. *Applied Computing and Informatics*, 17(2), 296–308. <https://doi.org/10.1016/j.aci.2018.10.001>
- Travassos, X. L., Pantoja, M. F., & Ida, N. (2021). Introduction to ground penetrating radar: Inverse Scattering and Data Processing. In *IEEE Press*. John Wiley & Sons, Inc. [https://doi.org/10.1049/pbce115e\\_ch1](https://doi.org/10.1049/pbce115e_ch1)
- Trevits, M., Monaghan, W., & Mucho, T. P. (2005). Assessment of Ground Conditions near a Mine Portal Using Ground Penetrating Radar. *24th International Conference on Ground Control in Mining*.
- Tsai, Y. J., Chou, Y. C., Wu, Y. S., & Lee, C. H. (2020). Noninvasive survey technology for LNAPL-contaminated site investigation. *Journal of Hydrology*, 587(March), 125002. <https://doi.org/10.1016/j.jhydrol.2020.125002>
- Tzanis, A. (2016). MATGPR: A freeware MATLAB package for the analysis of common-offset GPR data. *Geophysical Research Abstracts*, 8(March 2016).
- U.S. Energy Information Administration. (2021). Country analysis executive summary: Malaysia. In *Independent Statistic & Analysis*. <https://www.eia.gov/international/content/analysis/countrieslong/India/india.pdf>
- Ulugergerli, E. U., & Akca, I. (2006). Detection of cavities in gypsum. *The Journal of the Balkan Geophysical Society*, 9(1), 8–19. [http://www.balkangeophysoc.gr/online-journal/2006\\_V9/Dec2006/Vol\\_9\\_Dec\\_2006\\_p08-19\\_Ulugergerli.pdf](http://www.balkangeophysoc.gr/online-journal/2006_V9/Dec2006/Vol_9_Dec_2006_p08-19_Ulugergerli.pdf)
- Upadhyay, S., & Raghubanshi, A. S. (2020). Determinants of soil carbon dynamics in urban ecosystems. In *Urban Ecology*. Elsevier Inc. <https://doi.org/10.1016/b978-0-12-820730-7.00016-1>
- Utsi, E. C. (2017). Ground Penetrating Radar Theory and Practice. In *Ground Penetrating Radar Theory and Applications*. <https://doi.org/10.1016/B978-1-4160-5009-4.50004-2>
- Van Dam, R. L. (2014). Calibration Functions for Estimating Soil Moisture from GPR Dielectric Constant Measurements. *Communications in Soil Science and Plant Analysis*, 45(3), 392–413. <https://doi.org/10.1080/00103624.2013.854805>

- Vauclin, S., Mourier, B., Dendievel, A. M., Noclin, N., Piégay, H., Marchand, P., Vénisseau, A., de Vismes, A., Lefèvre, I., & Winiarski, T. (2021). Depositional environments and historical contamination as a framework to reconstruct fluvial sedimentary evolution. *Science of the Total Environment*, 764, 142900. <https://doi.org/10.1016/j.scitotenv.2020.142900>
- Vergnano, A., Godio, A., Raffa, C. M., Chiampo, F., Bosco, F., & Ruffino, B. (2019). Time-domain reflectometry (TDR) monitoring at a lab scale of aerobic biological processes in a soil contaminated by diesel oil. *Applied Sciences (Switzerland)*, 9(24). <https://doi.org/10.3390/app9245487>
- Verma, S., Gupta, M., & Misra, J. P. (2018). Performance evaluation of friction stir welding using machine learning approaches. *MethodsX*, 5(September), 1048–1058. <https://doi.org/10.1016/j.mex.2018.09.002>
- Vilbig, R. A. (2013). *Air-Coupled and Ground-Coupled Ground Penetrating Radar Techniques* (Issue August). Master Thesis. Northeastern University.
- Villavicencio, C. N., Macrohon, J. J. E., Inbaraj, X. A., Jeng, J. H., & Hsieh, J. G. (2021). Covid-19 prediction applying supervised machine learning algorithms with comparative analysis using weka. *Algorithms*, 14(7). <https://doi.org/10.3390/a14070201>
- Vlachou, M. C., Zacharias, K. A., Kostoglou, M., & Karapantsios, T. D. (2020). Droplet size distributions derived from evolution of oil fraction during phase separation of oil-in-water emulsions tracked by electrical impedance spectroscopy. *Colloids and Surfaces A*, 586(November 2019), 124292. <https://doi.org/10.1016/j.colsurfa.2019.124292>
- Wahab, S. (2013). *Assessing The Condition of Buried Pipe using Ground Penetrating Radar* (Issue August). University of Birmingham.
- Wang, P., Hu, Z., Zhao, Y., & Li, X. (2016). Experimental study of soil compaction effects on GPR signals. *Journal of Applied Geophysics*, 126, 128–137. <https://doi.org/10.1016/j.jappgeo.2016.01.019>
- Wang, T. P., Chen, C. C., Tong, L. T., Chang, P. Y., Chen, Y. C., Dong, T. H., Liu, H. C., Lin, C. P., Yang, K. H., Ho, C. J., & Cheng, S. N. (2015). Applying FDEM, ERT and GPR at a site with soil contamination: A case study. *Journal of Applied Geophysics*, 121, 21–30. <https://doi.org/10.1016/j.jappgeo.2015.07.005>

- Wang, Y., Feng, J., Lin, Q., Lyu, X., Wang, X., & Wang, G. (2013). Effects of crude oil contamination on soil physical and chemical properties in momoge wetland of China. *Chinese Geographical Science*, 23(6), 708–715. <https://doi.org/10.1007/s11769-013-0641-6>
- Waterland, L. R., Venkatesh, S., & Unnasch, S. (2003). *Safety and Performance Assessment of Ethanol/Diesel Blends (E-Diesel)* (Issue September). U.S. Department of Energy Laboratory.
- Waxman, M. H., & Thomas, E. C. (1974). Electrical Conductivities in Shaly Sands - I. The Relation Between Hydrocarbon Saturation and Resistivity Index; II. The Temperature Coefficient of Electrical Conductivity. *Journal of Petroleum Technology*, 26(55), 123–135. <https://doi.org/10.2118/4094-pa>
- Weihnacht, B., & Boerner, F. (2014). Measurement of retention functions with hysteresis using ground-penetrating radar. *Near Surface Geophysics*, 12(4), 539–548. <https://doi.org/10.3997/1873-0604.2014001>
- Wharton, R. P., Hazen, G. A., Rau, R. N., & Best, D. L. (1980). Electromagnetic Propagation Logging: Advances in Technique and Interpretation. *Society of Petroleum Engineers of AIME, (Paper) SPE*, 1–12. <https://doi.org/10.2118/9267-ms>
- Wijewardana, Y. N. S., Shilpadi, A. T., Mowjood, M. I. M., Kawamoto, K., & Galagedara, L. W. (2017). Ground-penetrating radar (GPR) responses for sub-surface salt contamination and solid waste: modeling and controlled lysimeter studies. *Environmental Monitoring and Assessment*, 189(2). <https://doi.org/10.1007/s10661-017-5770-4>
- Wilczek, A., Szyplowska, A., Lewandowski, A., Kafarski, M., Szerement, J., & Skierucha, W. (2018). Soil salinity characterization based on 0.05-3 GHz dielectric permittivity measurements. *2017 IEEE MTT-S International Microwave Workshop Series on Advanced Materials and Processes for RF and THz Applications, IMWS-AMP 2017, 2018-Janua*(September), 1–3. <https://doi.org/10.1109/IMWS-AMP.2017.8247431>
- Willmott, C. J., & Matsuura, K. (2005). Advantages of the mean absolute error (MAE) over the root mean square error (RMSE) in assessing average model performance. *Climate Research*, 30(1), 79–82. <http://www.jstor.org/stable/24869236>

- Wilson, V., Power, C., Giannopoulos, A., Gerhard, J., & Grant, G. (2009). DNAPL mapping by ground penetrating radar examined via numerical simulation. *Journal of Applied Geophysics*, 69(3–4), 140–149. <https://doi.org/10.1016/j.jappgeo.2009.08.006>
- Win, Z., Hamzah, U., Ismail, M. A., & Samsudin, A. R. (2011). Geophysical investigation using resistivity and GPR: A case study of an oil spill site at Seberang Prai, Penang. *Bulletin of the Geological Society of Malaysia*, 57(57), 19–25. <https://doi.org/10.7186/bgsm57201104>
- Wu, J. Bin, Tian, M., & Zhou, H. L. (2008). Feature extraction and recognition based on SVM. *2008 International Conference on Wireless Communications, Networking and Mobile Computing, WiCOM 2008*, 8–11. <https://doi.org/10.1109/WiCom.2008.483>
- Wu, T., Huang, R., Chi, M., & Weng, T. (2013). A study on electrical and thermal properties of conductive concrete. *Computers and Concrete*, 12(3), 337–349. <https://doi.org/10.12989/cac.2013.12.3.337>
- Wyszkowski, M., Wyszkowska, J., Borowik, A., & Kordala, N. (2020). Contamination of Soil with Diesel Oil, Application of Sewage Sludge and Content of Macroelements in Oats. *Water, Air, and Soil Pollution*, 231(11). <https://doi.org/10.1007/s11270-020-04914-2>
- Xie, X., Li, P., Qin, H., Liu, L., & Nobes, D. C. (2013). GPR identification of voids inside concrete based on the support vector machine algorithm. *Journal of Geophysics and Engineering*, 10(3). <https://doi.org/10.1088/1742-2132/10/3/034002>
- Xu, T. B. (2016). Energy harvesting using piezoelectric materials in aerospace structures. In *Structural Health Monitoring (SHM) in Aerospace Structures*. <https://doi.org/10.1016/B978-0-08-100148-6.00007-X>
- Yalcin, B., Amos, S. E., & Tangeman, J. (2015). Characterization. *Hollow Glass Microspheres for Plastics, Elastomers, and Adhesives Compounds*, 7–34. <https://doi.org/10.1016/B978-1-4557-7443-2.00002-5>
- Yamaguchi, T., & Mizutani, T. (2021). Detection and localization of manhole and joint covers in radar images by support vector machine and Hough transform. *Automation in Construction*, 126(October 2020), 103651. <https://doi.org/10.1016/j.autcon.2021.103651>



- Yelfm, R. J. (2007). Application of Ground Penetrating Radar to Civil and Geotechnical Engineering. *Electromagnetic Phenomena*, 7(No 1 (18)), 103–117.
- Yochim, A., Zytner, R. G., McBean, E. A., & Endres, A. L. (2013). Estimating water content in an active landfill with the aid of GPR. *Waste Management*, 33(10), 2015–2028. <https://doi.org/10.1016/j.wasman.2013.05.020>
- Yuan, H., Looms, M. C., & Nielsen, L. (2020). On the usage of diffractions in ground-penetrating radar reflection data: Implications for time-lapse gas migration monitoring. *Geophysics*, 85(5), H83–H95. <https://doi.org/10.1190/geo2019-0343.1>
- Yufryakov, B. A., & Linnikov, O. N. (2006). Buried cylinders geometric parameters measurement by means of GPR. *PIERS 2006 Cambridge - Progress in Electromagnetics Research Symposium, Proceedings*, 187–191. <https://doi.org/10.2529/piers051003234834>
- Zadhoush, H., Giannopoulos, A., & Giannakis, I. (2021). Optimising the complex refractive index model for estimating the permittivity of heterogeneous concrete models. *Remote Sensing*, 13(4), 1–15. <https://doi.org/10.3390/rs13040723>
- Zemo, D. A. (2006). Sampling in the smear zone: Evaluation of nondissolved bias and associated BTEX, MTBE, and TPH concentrations in ground water samples. *Ground Water Monitoring and Remediation*, 26(3), 125–133. <https://doi.org/10.1111/j.1745-6592.2006.00092.x>
- Zhang, X., Ma, Y., & Zhang, J. (2020). Shallow water bathymetry based on inherent optical properties using high spatial resolution multispectral imagery. *Remote Sensing*, 12(18). <https://doi.org/10.3390/RS12183027>
- Zhao, Y., Ling, D. sheng, Wang, Y. long, Huang, B., & Wang, H. lin. (2016). Study on a calibration equation for soil water content in field tests using time domain reflectometry. *Journal of Zhejiang University: Science A*, 17(3), 240–252. <https://doi.org/10.1631/jzus.A1500065>
- Zhou, L., Yu, D., Wang, Z., & Wang, X. (2019). Soil water content estimation using high-frequency ground penetrating radar. *Water (Switzerland)*, 11(5), 1–16. <https://doi.org/10.3390/w11051036>
- Zhu, X., Guo, W., & Wang, S. (2013). Sensing moisture content of buckwheat seed from dielectric properties. *Transactions of the ASABE*, 56(5), 1855–1862. <https://doi.org/10.13031/trans.56.10220>

## LIST OF PUBLICATIONS

### Journal with Impact Factor

1. **Ghazali, M. D.**, Zainon, O., Idris, K. M., Nor, S., Zainon, A., Karim, M. N. A., Anshah, S. A., & Talib, N. A. (2020). The Assessment of Relative Permittivity on Diesel Vapour in the Moisture Content of Terap Red Soil by Ground Penetrating Radar. *Air, Soil and Water Research*, 13, 1–11, <https://doi.org/10.1177/1178622120930661> (Q2, IF: 0.41)

### Indexed Conference Proceedings

1. **Ghazali, M. D.**, Zainon, O., Mohsin, R., Idris, K. M., & Mustafa, N. (2020). Estimated relative permittivity of contaminated laterite soil: An empirical model for GPR waves. *IOP Conference Series: Earth and Environmental Science*, 540(1). <https://doi.org/10.1088/1755-1315/540/1/012056> (Indexed by SCOPUS)
2. Halimshah, N. N., Yusup, A., Mat Amin, Z., & **Ghazali, M. D.** (2015). Visual Inspection Of Water Leakage From Ground Penetrating Radar Radargram. *ISPRS Annals of the Photogrammetry, Remote Sensing and Spatial Information Sciences*, 2(2W2), 191–198. <https://doi.org/10.5194/isprsannals-II-2-W2-191-2015> (Indexed by SCOPUS)

### List of Innovation Award

1. Gold Award  
Title: Modelling Dielectric Diesel Contamination in Laterite Soil on GPR  
International Innovation, Invention, Creation Exhibition, 2019.

2. Silver Award  
 Title: Empirical Model of Relative Permittivity for Diesel Contamination in Laterite Soil on the GPR  
 Ipoh International Summit on Professionalism, Research and Education, 2019.
3. Silver Award  
 Title: Disposable Hand Made Face Shield for Front Liners  
 The 5<sup>th</sup> International Innovation, Design and Articulation (IIDEA 2020)
4. Gold Award  
 Title: Disposal Hand Made Face Shield Front Liners  
 The 10th Seminar on Innovation and Creativity (SIC 2021)
5. Silver Award  
 Title: Disposal Hand Made Face shield  
 4<sup>th</sup> International Malaysia-Indonesia-Thailand Symposium on Innovation and Creativity (IMIT-SIC 2021)

#### **List of Grant Award**

1. Fundamental Research Grant Scheme (FRGS) -1/2021  
 Grant Award: RM103,848.00  
 Role: Leader  
 Title: Geo-Radar Signatures Segmentation for Laterite Soil Wastewater Tomography: Petrophysical Relationship and Cluttering Algorithms Model.
2. Fundamental Research Grant Scheme (FRGS) -1/2020  
 Grant Award: RM 91,800.00  
 Role: Member  
 Title: Geotechnical characterization based on antireflection meta surfaces technique for detection and characterization of sinkhole in Malaysia.